Acta Pharmaceutica Sinica B 2024;14(5):2153–2176

Chinese Pharmaceutical Association
Institute of Materia Medica, Chinese Academy of Medical Sciences

Acta Pharmaceutica Sinica B

www.elsevier.com/locate/apsb
www.sciencedirect.com

ORIGINAL ARTICLE

5*S*-Heudelotinone alleviates experimental colitis by shaping the immune system and enhancing the intestinal barrier in a gut microbiota-dependent manner

Qing Meng[a], Jianshuang Guo[a], Ke Lv[b], Yang Liu[a], Jin Zhang[a], Mingyue Li[a], Xirui Cheng[a], Shenghua Chen[b], Xiaoguang Huo[c], Quan Zhang[a,*], Yue Chen[a,b,*], Jing Li[a,b,*]

[a]*State Key Laboratory of Medicinal Chemical Biology, College of Pharmacy, Nankai University, Tianjin 300353, China*
[b]*College of Chemistry and Frontiers Science Center for New Organic Matter, Haihe Laboratory of Sustainable Chemical Transformations, Nankai University, Tianjin 300071, China*
[c]*Accendatech Company, Ltd., Tianjin 300193, China*

Received 6 September 2023; received in revised form 22 December 2023; accepted 19 January 2024

KEY WORDS

5*S*-heudelotinone;
Total synthesis;
Inflammatory bowel disease;
Gut microbiota;
Short-chain fatty acids;
Immune system;
Intestinal barrier;
Drug discovery

Abstract Aberrant changes in the gut microbiota are implicated in many diseases, including inflammatory bowel disease (IBD). Gut microbes produce diverse metabolites that can shape the immune system and impact the intestinal barrier integrity, indicating that microbe-mediated modulation may be a promising strategy for preventing and treating IBD. Although fecal microbiota transplantation and probiotic supplementation are well-established IBD therapies, novel chemical agents that are safe and exert strong effects on the gut microbiota are urgently needed. Herein, we report the total synthesis of heudelotinone and the discovery of 5*S*-heudelotinone (an enantiomer) as a potent agent against experimental colitis that acts by modulating the gut microbiota. 5*S*-Heudelotinone alters the diversity and composition of the gut microbiota and increases the concentration of short-chain fatty acids (SCFAs); thus, it regulates the intestinal immune system by reducing proinflammatory immune cell numbers, and maintains intestinal mucosal integrity by modulating tight junctions (TJs). Moreover, 5*S*-heudelotinone (**2**) ameliorates colitis-associated colorectal cancer (CAC) in an azoxymethane (AOM)/dextran sulfate sodium (DSS)-induced

*Corresponding authors.
E-mail addresses: zhangquan@nankai.edu.cn (Quan Zhang), yuechen@nankai.edu.cn (Yue Chen), jinglink@nankai.edu.cn (Jing Li).
Peer review under the responsibility of Chinese Pharmaceutical Association and Institute of Materia Medica, Chinese Academy of Medical Sciences.

https://doi.org/10.1016/j.apsb.2024.02.020

in situ carcinoma model. Together, these findings reveal the potential of a novel natural product, namely, 5*S*-heudelotinone, to control intestinal inflammation and highlight that this product is a safe and effective candidate for the treatment of IBD and CAC.

1. Introduction

Inflammatory bowel disease (IBD), which includes Crohn's disease (CD) and ulcerative colitis (UC), is a chronic relapsing disorder of the gastrointestinal (GI) tract that is characterized by persistent intestinal inflammation[1,2]. Diarrhea, bloody stool, abdominal pain, fatigue, and weight loss are common clinical symptoms of IBD and are related to poor quality of life and higher risk of developing colitis-associated colorectal cancer (CAC)[3,4]. Currently, the incidence and prevalence of IBD appear to be gradually increasing, and IBD is becoming a health problem worldwide[5]. The causes of IBD are complex and include genetic susceptibility, environmental exposure, disordered gut microbiota, dysregulated immune responses, and impaired intestinal mucosal barrier function[6,7]. Currently, anti-inflammatory drugs (such as amino salicylate and corticosteroids), antibiotics, and immunosuppressive drugs are the main clinical treatments for IBD[8]. However, these treatments are far from ideal, partly because they only alleviate symptoms and cause severe adverse effects. Hence, novel strategies or reagents that are both highly effective and safe are needed.

Although the etiology and pathogenesis of IBD remain largely unknown, recent studies have revealed that dysbiosis of the gut microbiota plays a pivotal role in IBD pathogenesis[9,10]. Significantly decrease in overall biodiversity, excessive growth of pathogenic bacteria, and reduced abundance of beneficial bacteria in the fecal microbiome have been observed in patients with IBD[11–13]. The gut microbiota contributes to host physiology by producing of a myriad of metabolites[14,15]. Short-chain fatty acids (SCFAs), mainly acetate, propionate and butyrate, are metabolites that are produced by the gut microbiota during dietary fiber fermentation in the intestinal tract[16]. The biological functions of SCFAs include shaping immune responses, promoting epithelial barrier function, maintaining intestinal barrier integrity, inhibiting the growth of harmful bacteria, and regulating tumor growth and development[17,18]. Decreased levels of SCFAs have been observed in patients with IBD and in experimental mouse models of IBD[19]. Therefore, the gut microbiota and related metabolites play important roles in the occurrence and development of IBD.

The gut microbiota and its metabolites can subsequently affect the immune balance in the intestines of IBD models by regulating both innate and adaptive immune cells[14,16]. Innate immune cells, such as macrophages and dendritic cells (DCs), can sense changes in the gut microbiota and rapidly induce inflammatory responses against invading microbes; additionally, SCFAs suppress proinflammatory cytokine production and promote the anti-inflammatory functions of immune cells to prevent excessive inflammatory responses[20–24]. Among adaptive immune disorders, imbalances in T helper type 17 (Th17) and regulatory T (Treg) cells are believed to be crucial for the development and progression of IBD[25]. Th17 cells, which are characterized by the secretion of large amounts of proinflammatory cytokines (such as IL-17A), play a central role in triggering exaggerated inflammatory responses in the intestine[26–28]. Treg cells are a specialized subpopulation of T cells that suppress the immune response by secreting anti-inflammatory cytokines, thereby maintaining homeostasis and self-tolerance[29,30]. Changes in the composition of the gut microbiota and SCFAs cause $CD4^+$ T cells to differentiate into Th17 cells, which contribute to the development of IBD[31,32]. In addition to regulating both innate and adaptive immune cells, SCFAs are the most important factors in the maintenance of intestinal epithelial integrity and the restoration of barrier function. The intestinal epithelium serves as a crucial physical barrier, bridging the gap between the gut microbiota and intestinal immune system[17,18,33]. Throughout this process, tight junctions (TJs), which are composed mainly of Claudins, Occludins and Zonula Occludens-1 (ZO-1), determine paracellular permeability[34]. Under normal physiological conditions, TJs interact with the commensal microbiome and intestinal immune system to maintain mucosal homeostasis. When the integrity of the physical barrier is impaired, detrimental microbial ligands or metabolites translocate into the gut and activate immune cells, leading to inflammatory responses[35,36]. Kelly et al.[37] reported that SCFAs, especially butyrate, play an important role in maintaining intestinal epithelial integrity and restoring barrier function. Butyrate enhances the expression of Claudin-1 and ZO-1, regulates the redistribution of Occludins and can also promote epithelial barrier function through IL-10 receptor-dependent repression of Claudin-2[38,39]. In summary, IBD involves a complex interaction among gut microbes, their metabolites (especially SCFAs), the epithelial barrier and the immune system. Therefore, modulation of the gut microbiota might be a promising strategy for IBD treatment.

Diterpenoids are among the most structurally diverse natural products, and many of them have shown promising effects in the treatment of inflammatory diseases in preclinical and clinical studies, such as rheumatoid arthritis, autoimmune diseases, asthma and IBD[40–45]. Therefore, diterpenoids may have potential therapeutic effects on inflammatory diseases. Icetexanes are natural diterpenoid products that are extracted from various *Salvia* specie[46]. These compounds have a [6,7,6]-tricyclic structure, which is believed to be constructed by the natural rearrangement of the more commonly found [6,6,6]-fused abietane diterpenoids. Norditerpenoids, a specific type of diterpenoid, are relatively rare in nature. Furthermore, few reports have described norditerpenoids with a [6,7,6]-tricyclic ring. Herein, some isolated norditerpenoids with [6,7,6]-tricyclic ring are summarized in Fig. 1. These norditerpenoids were extracted from plants such as *Ricinodendron heudelotii*, *Trigonostemon chinensis*, and *Flueggea virosa*[47–49]. However, there have been limited reports on their synthesis, biological properties, and potential pharmaceutical applications; thus, there are significant opportunities for further study on norditerpenoids. Heudelotinone (12-hydroxy-3-oxo-9(10→20)-abeo-16,17-dinor-abieta-1(2),8, 10(20),11,13-pentaene) is an icetexane-type dinorditerpenoid featuring a [6,7,6]-tricyclic core. In 1991, Connolly et al. first

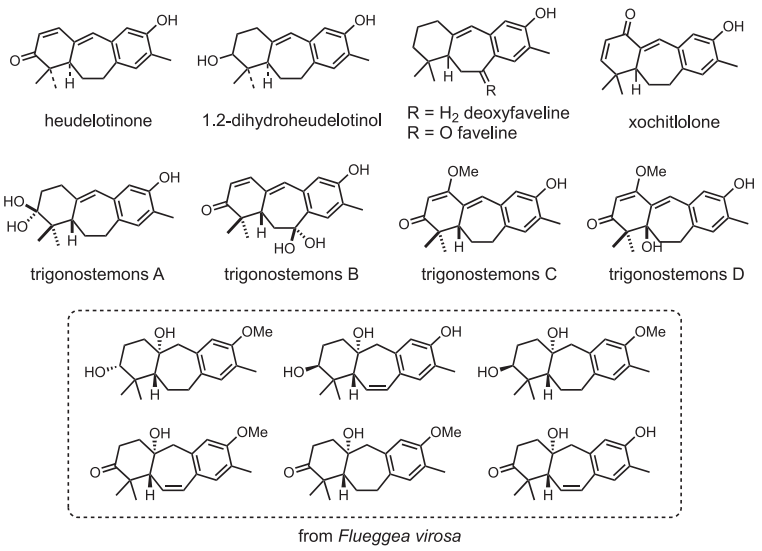

Figure 1 Icetexane-type norditerpenoid natural products.

isolated heudelotinone from the stem bark and roots of *R. heudelotii*[47] and determined its structure. Subsequently, many other research groups also extracted and isolated heudelotinone from *Jatropha curcas*, *T. chinensis*, *Trigonostemon xyphophylloides* and *Jatropha multifida*[49−52]. However, heudelotinone is present at low levels in the plants of origin, and only 20 mg of heudelotinone can be extracted from 15 kg of bark; thus, it is difficult to obtain heudelotinone in large quantities by traditional extraction and separation methods[49,50,53], which makes it impossible to conduct *in vivo* pharmacological evaluations. Accordingly, it is of great value to synthesize heudelotinone in large quantities and elucidate its pharmacological mechanism.

Herein, we report for the first time the total synthesis of the racemate of the natural product heudelotinone *via* a simple and efficient manner that yields gram-level quantities. A pair of enantiomers, namely, 5*R*-heudelotinone (**1**) and 5*S*-heudelotinone (**2**), are obtained by chiral resolution *via* chiral high-performance liquid chromatography (HPLC). Next, we demonstrate that 5*S*-heudelotinone (**2**) exhibits potent effects against dextran sulfate sodium (DSS)-induced colitis and that the underlying mechanism depends on the gut microbiota. Moreover, 5*S*-heudelotinone (**2**) regulates the diversity and composition of the gut microbiota, increases the proportion of beneficial bacteria, decreases the abundance of pathogenic bacteria, and improves the levels of SCFAs. Further analysis revealed that 5*S*-heudelotinone (**2**) could reduce the populations of various immune cells, including macrophages, DCs, myeloid-derived suppressor cells (MDSCs) and Th17 cells, and simultaneously promote the integrity of the intestinal mucosa by maintaining intestinal TJ integrity in a DSS-induced mouse colitis model; moreover, these effects are all mediated *via* the gut microbiota. Additionally, treatment with 5*S*-heudelotinone (**2**) ameliorates ongoing colitis and inhibits the occurrence and development of CAC in an azoxymethane (AOM)/DSS-induced *in situ* carcinoma model. Together, our findings reveal a novel candidate for the treatment of IBD and provide a unique perspective on innovative IBD drug discovery.

2. Materials and methods

2.1. Chemicals

Commercially available chemical reagents and solvents were purchased from different high-quality reagent companies and were used without further purification. All air-sensitive reactions were performed under an atmosphere of argon, and the solvents were dried by distillation over Na. Thin layer chromatography (TLC) was used to monitor the reactions on silica gel plates. Column chromatography was performed on silica gel with 200−300 mesh. ^{1}H NMR and ^{13}C NMR spectra were recorded with a Bruker Avance 400, and the data were reported in the following form: chemical shift (referenced to residual solvent peaks ($CDCl_3$ ^{1}H NMR = 7.26 ppm, ^{13}C NMR = 77.16 ppm; CD_3OD ^{1}H NMR = 3.31 ppm, ^{13}C NMR = 49.00 ppm) or to $Si(CH_3)_4$ as an internal standard), multiplicity (s = singlet, d = doublet, t = triplet, q = quartet, m = multiplet), coupling constants (quoted in Hz) and integration. High-resolution mass spectra (HRMS) were detected with an IonSpec QFT mass spectrometer with ESI ionization. Determination of specific optical rotations was recorded with an Insmark IP 120 digital polarimeter.

2.2. Animals

C57BL/6J (wild type; WT) mice (male, 6−8 weeks old, 20−22 g) and Sprague−Dawley rats (male, 6−8 weeks old, 180−220 g) were purchased from Beijing Vital River Laboratory Animal Technology Co., Ltd. The mice were maintained under specific pathogen-free conditions with a 12 h light-dark cycle. All the animal experiments were performed in accordance with the Regulations for the Administration of Affairs Concerning Experimental Animals (Tianjin, revised in June 2018) and in compliance with the Guiding Principles in the Care and Use of Animals of the American Physiological Society, and the animal experiments were approved by the Institutional Animal Care and Use Committee

(IACUC) of Nankai University (Tianjin, China, No. 2023-SYDWLL-000537).

2.3. DSS-induced experimental colitis and treatment

The experimental procedures were as follows:

I) To investigate the protective effect of 5*S*-heudelotinone (**2**), 40 mice were randomly divided into 4 groups ($n = 10$): a Control group, DSS group, low-dose group (50 mg/kg) and high-dose group (100 mg/kg). To induce acute experimental colitis, the mice were administered 3% (*w*/*v*) DSS (molecular weight of 36,000−50,000 Da; MP Biomedicals, UK) dissolved in their drinking water for 10 days. 5*S*-Heudelotinone (**2**) was suspended in 10% DMSO + 90% maize oil, and mice in each treatment group received the corresponding dose of 5*S*-heudelotinone (**2**) *via* intragastric (i.g.) administration once per day. Moreover, mice in the Control and DSS groups were given the same volume of solvent *via* i.g. administration. The body weight and pathological features of each mouse were evaluated daily. The disease activity index (DAI) was determined and recorded daily to quantify colitis severity as previously described.

II) To investigate the central role of the gut microbiota in the amelioration of colitis by 5*S*-heudelotinone (**2**), 30 mice were stochastically divided into 3 groups ($n = 10$): an ABX group, ABX + DSS group and ABX + DSS+**2** group. All the mice were administered broad-spectrum antibiotic cocktails (including 1 mg/mL ampicillin (J&K, A01-290395), 1 mg/mL metronidazole (J&K, J07-M0924), 0.5 mg/mL vancomycin (INALCO, 1758−9326) and 1 mg/mL neomycin (J&K, A01-557926)) for 5 days to deplete the resident microbiome of the intestine. Then, 2% DSS was administered for 7 days to induce experimental colitis due to the enhanced sensitivity of gut microbiota-depleted mice to DSS. 5*S*-Heudelotinone (**2**) was administered throughout the whole process.

III) In the therapeutic experiment, colitis was induced by administering 3% DSS in drinking water for 7 days, and then, the mice were given normal drinking water for the remaining days. The mice were administered 5*S*-heudelotinone (**2**) by gavage beginning on Day 7 and continuing until they were euthanized.

2.4. Quantitative RT-PCR

Total RNA was extracted from mouse colon tissues using TRIzol (TaKaRa) and transcribed to cDNA using All-in-one cDNA Synthesis Supermix (TransGene Biotech). Real-time PCR analysis was performed using *PerfectStart* Green qPCR MasterMix (TransGene Biotech) according to the manufacturer's protocol. The results were normalized to the expression of a housekeeping gene. The primer sequences are listed in Table S2.

2.5. Western blotting analysis

Cells or colon tissue samples were lysed in RIPA buffer (Beyotime, Shanghai, China) supplemented with protease inhibitors for 30 min on ice. The homogenates were centrifuged at 11,000 rpm for 20 min at 4 °C. The total protein concentrations in the supernatants were quantified by the BCA assay (Thermo Fisher Scientific, Waltham, MA, USA). Protein samples with equal concentrations were separated in SDS-PAGE gels and transferred to PVDF membranes (Bio-Rad). After blocking with 5% BSA for 2 h, the membranes were incubated at 4 °C overnight with primary antibodies against the following target proteins: TNF-α (ABclonal, A11534, dilution 1:1000), IL-6 (ABclonal, A0286, dilution 1:1000), IL-1β (ABclonal, A16288, dilution 1:1000), COX2 (Abcam, ab79393, dilution 1:1000), iNOS (Abcam, ab178945, dilution 1:1000), β-Actin (Proteintech, CL594-66009, dilution 1:5000), GAPDH (Abways, AB0037, dilution 1:5000), Claudin-2 (Abcam, ab53032, dilution 1:1000), Claudin-4 (Abcam, ab15104, dilution 1:1000), Claudin-7 (Abcam, ab27487, dilution 1:1000), ZO-1 (Abcam, ab96587, dilution 1:1000), and Occludin (Abcam, ab216327, dilution 1:1000). After washing, the membranes were incubated with the corresponding secondary antibodies for 2 h at room temperature (RT). The immune complexes were detected with an ECL reagent (Thermo Fisher Scientific, Waltham, MA, USA).

2.6. Measurement of cytokine levels by enzyme-linked immunosorbent assay (ELISA)

Proteins were extracted from distal colons of healthy and DSS-induced IBD mice treated with or without 5*S*-heudelotinone (**2**). The concentrations of TNF-α and IL-6 were quantified by enzyme-linked immunosorbent assay following the manufacturer's instructions (Biolegend, CA, USA). The absorbance was determined at 450 nm using a microplate reader (Bio-Rad, iMark, USA).

2.7. Fecal genomic DNA extraction and 16S-rRNA gene sequencing

Total genomic DNA samples were extracted using the Omega Mag-bind Soil DNA Kit (M5636-02) (Omega Bio-Tek, Norcross, GA, USA) following the manufacturer's instructions and stored at −20 °C prior to further analysis. The quantity and quality of the extracted DNA were measured using a NanoDrop NC2000 spectrophotometer (Thermo Fisher Scientific, Waltham, MA, USA) and agarose gel electrophoresis, respectively. PCR amplification of the bacterial 16S rRNA gene V3−V4 region was performed with the forward primer 338F (5′-ACTCCTACGGGAGGCAGCA-3′) and the reverse primer 806R (5′-GGACTACHVGGGTWTCTAAT-3′). Sample-specific 7-bp barcodes were incorporated into the primers for multiplex sequencing. The PCR solutions included 5 μL of buffer (5 ×), 0.25 μL of Fast pfu DNA Polymerase (5 U/μL), 2 μL (2.5 mmol/L) of dNTPs, 1 μL (10 μmol/L) of each forward and reverse primer, 1 μL of DNA template, and 14.75 μL of ddH_2O. The thermal cycling conditions included initial denaturation at 98 °C for 5 min, followed by 25 cycles of denaturation at 98 °C for 30 s, annealing at 53 °C for 30 s, and extension at 72 °C for 45 s, with a final extension of 5 min at 72 °C. The PCR amplicons were purified with Vazyme VAHTSTM DNA Clean Beads (Vazyme, Nanjing, China) and quantified using the Quant-iT PicoGreen dsDNA Assay Kit (Invitrogen, Carlsbad, CA, USA). After individual quantification step, the amplicons were pooled in equal amounts, and pair-end 2 × 250 bp sequencing was performed using the Illumina NovaSeq platform with a NovaSeq 6000 SP Reagent Kit (500 cycles) at Suzhou PANOMIX Biomedical Tech Co., Ltd.

2.8. Targeted SCFA quantitative analysis

In this experiment, 100 mg/mL mixed standard stock solutions of 6 SCFAs (acetic acid, propionic acid, isobutyric acid, butyric acid, isovaleric acid and valeric acid) and 100 mg/mL caproic acid

stock solution were prepared in water and ether, respectively. The 6 SCFAs and caproic acid working solutions were both prepared by dilution in the appropriate standard stock solution. Then, 375 μg/mL internal standard (IS) solution containing 4-methylvaleric acid was similarly prepared with ether. Fecal samples were homogenized for 1 min with 500 μL of water and 100 mg of glass beads, and then these samples were centrifuged at 4 °C for 10 min at 12,000 rpm. Then, 200 μL of supernatants were extracted with 100 μL of 15% phosphoric acid, 20 μL of 4-methylvaleric acid solution (375 μg/mL) as the IS, and 280 μL of ether. Subsequently, the samples were centrifuged at 4 °C for 10 min at 12,000 rpm after vortexing for 1 min, and the supernatants were transferred to a vial prior to GC−MS analysis. Then, GC analysis was performed on a trace 1300 gas chromatograph (Thermo Fisher Scientific, USA). The GC was fitted with an Agilent HP-INNOWAX capillary column (30 mm × 0.25 mm ID × 0.25 μm), and helium was used as the carrier gas and delivered at 1 mL/min. Samples were injected in split mode at 10:1 in an injection volume of 1 μL and at an injector temperature of 250 °C. The temperatures of the ion source and MS transfer line were 300 and 250 °C, respectively. The column temperature was programmed as follows: an initial temperature of 90 °C, followed by an increase to 120 °C at 10 °C/min, an increase to 150 °C at 5 °C/min, and finally an increase to 250 °C at 25 °C/min, and this final temperature was maintained for 2 min. Mass spectrometric detection of metabolites was performed with an ISQ 7000 (Thermo Fisher Scientific, USA) in electron impact ionization mode. Single ion monitoring (SIM) mode was used with an electron energy of 70 eV.

2.9. AOM/DSS-induced CRC model

C57BL/6J mice were administered a single intraperitoneal injection of AOM (Sigma−Aldrich, USA) at a dose of 10 mg/kg as previously described[54]. One week later, the mice were subjected to 3 cycles of 2% DSS administration for 7 days followed by regular sterile water for 14 days. During each cycle, the mice received different doses of 5*S*-heudelotinone (**2**) (50 and 100 mg/kg) continuously for the first 2 weeks. The mice were sacrificed on Day 84. The lengths of the colon and intestine were measured, and the tumor number and size in each mouse were counted and recorded. Colonic tissues were collected to generate Swiss rolls and processed for hematoxylin and eosin (H&E) and Ki67 staining.

2.10. Immunohistochemistry and immunofluorescence analysis

In brief, a 1-cm segment of the distal colon was fixed with 4% paraformaldehyde and embedded in paraffin, and 4-μm-thick sections were stained with H&E according to standard protocols. Colonic pathology was evaluated based on a previously described histological scoring system. For immunohistochemistry, the sections were stained with an antibody against Ki67 (Boster Biological Technology, A00254, China) overnight at 4 °C. For immunofluorescence, the sections were stained with antibodies against Occludin (Abcam, ab216327, dilution 1:100) and ZO-1 (Abcam, ab96587, dilution 1:200). For cell death analysis, terminal deoxynucleotidyl transferase dUTP nick end labeling (TUNEL) staining was performed using the One Step TUNEL Apoptosis Assay Kit (Beyotime, Cat. No. C1088, China) according to the manufacturer's protocol.

2.11. Isolation of intestinal immune cells

Colon tissues were first incubated in preheated Ca/Mg-free Hanks' balanced salt solution (HBSS, BasalMedia, B430KJ) with 5 mmol/L EDTA (Solarbio), 1 mmol/L dithiothreitol (Biosharp, BS110) and 5% fetal bovine serum twice for 20 min each with shaking to remove the mucus and intestinal epithelial cells. After washing with complete HBSS, the colon tissues were then digested in complete medium supplemented with 2 mg/mL Collagenase IV (Biosharp, BS165) for 1 h at 37 °C with shaking. The supernatants were filtered through 70-μm cell strainers and resuspended in FACS buffer. After centrifugation for 10 min, intestinal immune cells were obtained.

2.12. Isolation of splenic immune cells

Spleen tissues were first ground and filtered through cell strainers. The supernatants were then discarded after centrifugation. The splenic cells were added to ACK lysis buffer (Solarbio, R1010) and incubated for 30 min. After centrifugation for 5 min, the splenic immune cells were obtained.

2.13. Flow cytometry

For cell surface antigen staining, cells were preincubated with FcR Blocking Reagent (BioLegend) for 30 min at 4 °C before being stained with antibodies. The cells were stained with mouse antibodies against the following target proteins: CD45 (FITC, BioLegend, lot 103108, clone 30-F11, dilution 1:100), CD4 (PE, BioLegend, lot 100407, clone GK1.5, dilution 1:100), CD3ε (PerCP/Cyanine5.5, BioLegend, lot 100328, clone 145-2C11, dilution 1:100), IL-17A (APC, BioLegend, lot 506915, clone TC11-18H10.1, dilution 1: 100), FOXP3 (Alexa Fluor® 647, BioLegend, lot 320013, clone 150D, dilution 1:100), CD11b (PE, BioLegend, lot 101208, clone M1/70, dilution 1:100), F4/80 (APC, BioLegend, lot 123116, clone BM8, dilution 1:100), I-A/I-E (APC, BioLegend, lot 107614, clone M5/114.15.2, dilution 1:100), Gr-1 (APC, BioLegend, lot 108412, clone RB6-8C5, dilution 1:100), and CD11c (PE, BioLegend, lot 117307, clone N418, dilution 1:100). Flow cytometry was performed using a BD LSR Fortessa. The data were analyzed using FlowJo software.

2.14. Acute toxicity assay

For the acute toxicity study of 5*S*-heudelotinone (**2**), C57/6J mice were fasted for 12 h and then intragastrically administrated with different dosages of 5*S*-heudelotinone (**2**) (500 and 1000 mg/kg) once. Body weighs were measured every other day. Each group consisted of 10 mice (5 males and 5 females).

2.15. Subacute toxicity assay

For the subacute toxicity study of 5*S*-heudelotinone (**2**), C57/6J mice were fasted for 12 h and then intragastrically administrated with different dosages of 5*S*-heudelotinone (**2**) (100 and 200 mg/kg) daily for 14 days. Body weighs were measured every other day. Each group consisted of 10 mice (5 males and 5 females). To evaluate the biosafety of 5*S*-heudelotinone (**2**), blood samples were collected for blood routine assay and blood biochemical assay. Major organs, including heart, liver, spleen, lung, and kidney, were collected and stained with H&E for histopathologic analysis.

2.16. Pharmacokinetics (PK) study

Six male Sprague−Dawley rats were randomly divided into two groups to receive intravenous (2 mg/kg) or oral administration (20 mg/kg) of 5*S*-heudelotinone (**2**). Blood samples of each group were collected from retrobulbar venous plexus at 5, 15, 30 min, 1, 2, 4, 6, 8, 12 and 24 h post-dose into heparinized tubes. Plasma was obtained after centrifugation and stored at −20 °C until they were analyzed. In this study, UPLC−MS/MS analysis was carried out on an Ultra performance liquid chromatographic system (Shimadzu, Japan). The chromatographic column was Synergi Fusion-RP 80A LC Column (50 mm × 2 mm, 4 μm). Mass spectrometric detection was performed on API 4000 mass spectrometer with an electrospray ionization (ESI) interface operating in positive ion mode, was manufactured by SCIEX (Framingham, USA). The MS/MS system was operated at unit resolution in the multiple reaction monitoring (MRM) mode, and the monitored transitions were *m/z* 269.2 → 210.7 for 5*S*-heudelotinone (**2**). The plasma concentration−time profiles of 5*S*-heudelotinone (**2**) were plotted.

2.17. Liver microsomal metabolic stability study

A solution of 5*S*-heudelotinone (**2**) (1 mmol/L final concentration) was incubated in a 100 mmol/L potassium phosphate buffer solution (pH 7.4) containing human or rat liver microsomes (HLMs, BioIV, X008070; RLMs, Rild-biotech, LM-DS-02M, 0.5 mg/kg), the enzyme cofactor nicotinamide adenine dinucleotide phosphate (NADPH, Solarbio, N8100, 1 mmol/L) and 5 mmol/L $MgCl_2$. A negative control without NADPH was also performed in parallel to assess any chemical instability or non-NADPH dependent enzymatic degradation. Verapamil (Sigma, V4629) was used as positive control for metabolism across species. Time points were taken at 0, 15, 30, 60, 90 and 60 min by adding acetonitrile with internal standard tolbutamide (Sigma, T0891) to stop the reaction. Samples were vortexed for 2−3 min and then centrifuged at 15,000 rpm for 10 min. An aliquot of the supernatant (100 μL) was mixed with 100 μL ultra-pure water prior to analysis. The concentrations of 5*S*-heudelotinone (**2**) in the samples were determined by UPLC−MS/MS. The intrinsic clearance (CL_{int}) and half time ($t_{1/2}$) were calculated. In this study, UPLC−MS/MS analysis was carried out on an Ultra performance liquid chromatographic system (ExionLC, SCIEX, USA). The chromatographic column was Waters CORTECS® C18+ (2.1 mm × 50 mm, 2.7 μm). Mass spectrometric detection was performed on Triple QuadTM 4500 mass spectrometer with an electrospray ionization (ESI) interface operating in positive ion mode, was manufactured by SCIEX (Framingham, USA). The MS/MS system was operated at unit resolution in the multiple reaction monitoring (MRM) mode, and the monitored transitions were *m/z* 269.1 → 211.1 for 5*S*-heudelotinone (**2**).

2.18. Statistical analysis

All results are shown as the mean ± SEM as indicated. Levels of significance for comparisons between two groups were evaluated with unpaired two-tailed Student's *t* test and one- or two-way analysis of variance (ANOVA) of comparison of multiple groups. GraphPad Prism 9.0 software was used for statistical analysis. Statistical significance is indicated as follows: $^{\#}P < 0.05$, $^{\#\#}P < 0.01$, $^{\#\#\#}P < 0.001$, $^{*}P < 0.05$, $^{**}P < 0.01$, $^{***}P < 0.001$, $^{+}P < 0.05$ and $^{++}P < 0.01$, and n.s. indicates no significance. For the quantification of Western blotting results, the bands were quantified by ImageJ software.

3. Results

3.1. Total synthesis of heudelotinone

The strategy for synthesizing the [6+7+6] ring system in heudelotinone was designed to proceed as shown in Scheme 1, making use of the Diels−Alder (DA) reaction to join two readily available fragments, namely, Danishefsky-type diene **4** and dienophilic substrate **5**. Intermediate **5** could be elaborated from known compound **6**.

Our investigation started by preparing **5** from known compound **6** in 79% yield over two steps, namely, silyl enol ether formation and IBX oxidation, and Danishefsky-type diene **4** was obtained in three steps according to a previously reported method[55]. With intermediates **4** and **5** in hand, we poised to explore the key DA reaction to furnish the desired [6+7+6] ring system[56]. Initially, a Lewis acid was supposed to form a complex with a dienophilic substrate to promote the DA reaction. Under a variety of Lewis acid conditions, such as zinc chloride, zinc bromide, dimethyl aluminum chloride, tin dichloride, and diethyl aluminum chloride, no reaction was observed or the starting material decomposed into a complex mixture. Interestingly, when boron trifluoride ether was applied, dione **8** was obtained in 75% yield, but the desired product **8a** was not detected. Next, we

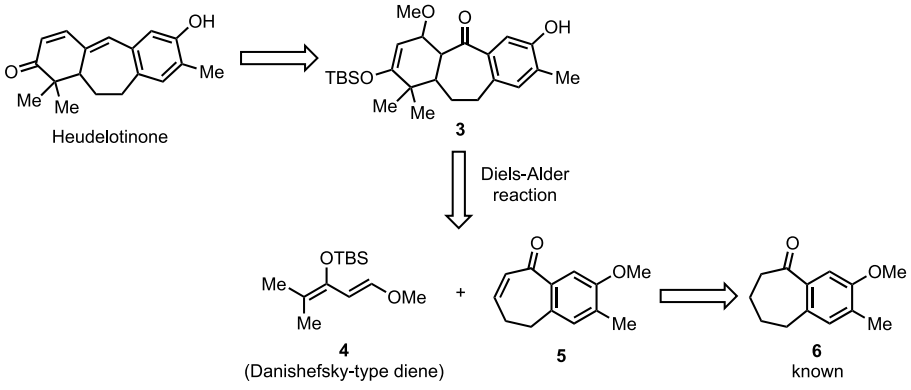

Scheme 1 Retrosynthetic analysis of heudelotinone.

planned to synthesize **10** from **8** in three steps (double-bond shift, reduction and elimination). Primarily, we aimed to obtain compound **9a** from **8** under the treatment of *p*-TsOH in methanol. However, a 49% yield of product **9** and a nearly equal amount of **9′** were generated. Then, compound **9** was expected to produce alcohol **10a** under the treatment of LAH in THF. Fortunately, the desired product ketone **10** was directly generated. This transformation presumably occurred due to the instability of reduction product **10a**, which underwent an elimination reaction to yield **10** during the heating and concentration processes. Eventually, **10** was subjected to demethylation using boron tribromide, producing product **11** in a yield of 92% (Scheme 2). The ^{1}H NMR data, ^{13}C NMR data, and other analytic data of synthesized product **11** were identical to those of the reported naturally occurring heudelotinone. Herein, an efficient route for synthesizing heudelotinone with a yield of 5 g was developed.

Since the absolute configuration of heudelotinone has not yet been reported, we separated compound **11** *via* chiral HPLC and obtained two corresponding enantiomers (Supporting Information Figs. S36 and S37, Table S3). Next, we verified the structures and absolute configurations of the two separated components. First, we measured the specific rotation of **11**, components 1 and 2. As shown in Supporting Information Table S4, the specific rotation of compound **11** was 0, and components 1 and 2 were a pair of corresponding enantiomers with opposite optical activities. Finally, the absolute configurations of the two enantiomers were determined by X-ray crystallographic diffraction analysis; the results revealed that component 1 was in the *R* configuration and component 2 was in the *S* configuration, namely, 5*R*-heudelotinone (**1**) and 5*S*-heudelotinone (**2**), respectively (Supporting Information Tables S5 and S6).

3.2. 5*S*-Heudelotinone delays the onset of colitis

Most terpenoids have anti-inflammatory activities, and the plants of origin (*J. curcas* and *Trigonostemon howii*) for heudelotinone also exert anti-inflammatory effects and are used to treat diarrhea[53,57]. Hence, to investigate whether 5*R*-heudelotinone (**1**) and 5*S*-heudelotinone (**2**) inhibit the inflammatory response during the development of IBD, we first treated healthy C57BL/6J mice with compound **1** or **2** by gavage at a dosage of 100 mg/kg once per day (Supporting Information Fig. S1A). Over 11 days, no evident clinical or histological abnormalities were observed in terms of body weight (Fig. S1B–S1E), colon length (Fig. S1F and S1G), histopathology (Fig. S1H) or spleen tissue (Fig. S1I and S1J), indicating that at this dosage and in this solvent, neither compound was toxic. Next, we treated C57BL/6J mice with 5*R*-heudelotinone (**1**) and 5*S*-heudelotinone (**2**) when establishing a DSS-induced acute experimental colitis model, which is widely used because its clinical and pathological features are similar to those of human UC. Mice were administered 3% DSS in their drinking water for 9 days, and **1** or **2** suspended in 10% DMSO +90% maize oil was synchronously administered *via* the i.g. route at a dosage of 50 mg/kg once per day (Supporting Information Fig. S2A). We found that both preventive compounds **1** and **2** attenuated experimental colitis by improving the body weight, DAI score, colon length, pathology and spleen weight of the mice, and the effect of compound **2** was better than that of **1** (Fig. S2B–S2J).

To further investigate the effect of 5*S*-heudelotinone (**2**) on the development of IBD, we treated mice with 5*S*-heudelotinone (**2**) at two different doses once per day after the acute colitis model was successfully established as mentioned above (Fig. 2A). 5*S*-Heudelotinone (**2**) significantly ameliorated the DSS-induced decrease in

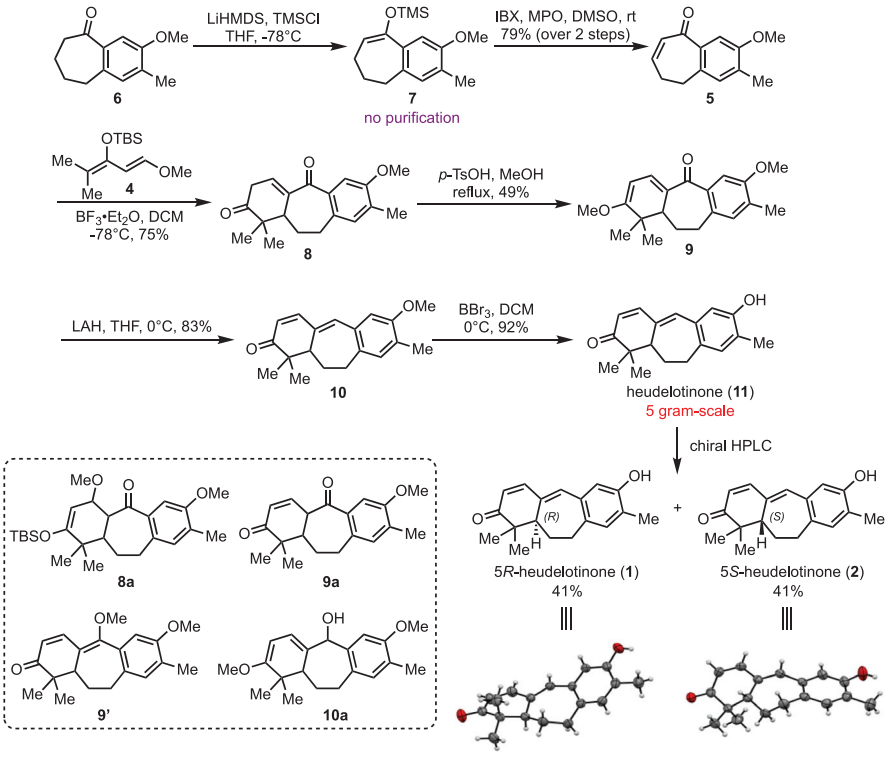

Scheme 2 Total synthesis of heudelotinone. LiHMDS = lithium hexamethyldisilazide, TMSCl = *t*-butyldimethylchlorosilane, IBX = 2-iodoxybenzoic acid, MPO = 4-methoxypyridine-*N*-oxide, *p*-TsOH = *p*-toluenesulfonic acid, LAH = lithium aluminum hydride, BBr_3 = boron tribromide.

body weight in a dose-dependent manner (Fig. 2B). Moreover, the DAI was also decreased after the administration of 5*S*-heudelotinone (**2**) (Fig. 2C). Shortened colon length and increased spleen weight are symptoms of DSS-induced colitis. Compared with the DSS group, we observed marked relief of colonic shortening and splenomegaly in the 5*S*-heudelotinone (**2**)-treated groups (Fig. 2D and E, Supporting Information Fig. S3). H&E staining of colon tissue sections showed that the mice in the DSS group presented severe pathology, as evidenced by widely disrupted crypt architecture, great reductions of goblet cell numbers, severe mucosal damage, abundant inflammatory cell infiltration and higher histology scores. In contrast, 5*S*-heudelotinone (**2**) treatment significantly ameliorated these symptoms, and these mice exhibited well-preserved crypt architectures, limited inflammation, intact mucosal structure, and lower histology scores (Fig. 2F and G). To further verify the protective effect of 5*S*-heudelotinone (**2**) on the intestinal mucosa, we carried out a TUNEL assay. The results demonstrated that treatment with 5*S*-heudelotinone (**2**) resulted in significant decrease in apoptosis, especially in the high-dose group (Fig. 2H and I). Furthermore, excessive secretion of proinflammatory cytokines is closely related to intestinal inflammation and the clinical symptoms of IBD. Therefore, we assessed the levels of proinflammatory cytokines, including TNF-α, IL-6 and IL-1β. As expected, 5*S*-heudelotinone (**2**) led to a profound reduction in the levels of these cytokines, as determined by RT-qPCR, ELISA and immunoblotting analysis (Fig. 2J−Q). Additionally, we also found that the expression of two inducible enzymes that are associated with inflammation, namely, iNOS and COX-2, was restored to the level observed in the Control group after treatment with 5*S*-heudelotinone (**2**) (Fig. 2M and P); these results indicated that 5*S*-heudelotinone (**2**) weakened the inflammatory response during the development of colitis. Taken together, these findings suggest that treatment with 5*S*-heudelotinone (**2**) can effectively delay the onset of colitis and preemptively alleviate the symptoms of colitis.

Moreover, in an acute toxicity study of 5*S*-heudelotinone (**2**), mice tolerated intragastric administration of 5*S*-heudelotinone (**2**) at dosages up to 1000 mg/kg. No mice died within 2 weeks, and no behavioral abnormality (*i.e.*, lethargy, clonic convulsion, anorexia, or ruffled fur) were observed in the treated animals. In addition, there was no significant difference in weight change between the 5*S*-heudelotinone (**2**)-treated groups and the Control group for both genders over a 2-week period ($P > 0.05$) (Supporting Information Fig. S4). Meanwhile, a subacute toxicity study of 5*S*-heudelotinone (**2**) demonstrated that no deaths or abnormal behaviors were observed among the treated mice. The body weight changes of mice in each group showed no statistically significant differences compared with the Control group in each gender ($P > 0.05$) (Supporting Information Fig. S5A and S5B). As well as blood routine assays, blood biochemical assays were performed to evaluated the biosafety of 5*S*-heudelotinone (**2**). As shown in Fig. S5C−S5I, there was no obvious changes of the values of red blood cells (RBC), mean corpuscular hemoglobin concentration (MCHC), red blood cell-specific volume (HCT), mean corpuscular volume (MCV), platelets (PLT), red blood cell volume distribution width (RDW), and mean platelet volume (MPV) in the mice treated with 5*S*-heudelotinone (**2**). Moreover, no obvious increases in indicators including alkaline phosphatase (ALP), alanine transaminase (ALT), aspartate transaminase (AST), creatinine (CRE), and blood urea nitrogen (BUN) demonstrated no apparent kidney or liver damage arising from 5*S*-heudelotinone (**2**) (Fig. S5J−S5N). In addition, we also carried out hematoxylin and eosin staining of vital organs (*i.e.*, heart, liver, spleen, lung, and kidneys) for histopathological examination. Accordingly, no marked signs of inflammation or histopathological abnormalities were found (Supporting Information Fig. S6), further proving that 5*S*-heudelotinone (**2**) did not have a negative impact on major organs and may be safe for the *in vivo* treatment of experimental colitis.

3.3. 5*S*-Heudelotinone alleviates colitis in a gut microbiota-dependent manner

The preliminary pharmacokinetic study of 5*S*-heudelotinone (**2**) indicated a poor oral bioavailability. Moreover, 5*S*-heudelotinone (**2**) exhibited relative low stability in HLMs and RLMs with $t_{1/2}$ = 28.66 and 2.38 min, respectively. However, we discovered that 35.51%−66.59% of 5*S*-heudelotinone (**2**) was directly excreted through the intestines (Supporting Information Figs. S7 and S8 and Table S1). Therefore, we speculate that 5*S*-heudelotinone (**2**), through gut microbiota, makes the host resistant to colitis. To investigate whether the protective effect of 5*S*-heudelotinone (**2**) against colitis depends on the gut microbiota, a gut microbiota-depleted mouse model was established by administering a quadruple antibiotic cocktail (ABX) for 5 days before DSS treatment (Fig. 3A). Notably, the effect of 5*S*-heudelotinone (**2**) on mitigating disease was abrogated when the gut microbiota was eliminated by ABX, as evidenced by the indistinguishable body weight (Fig. 3B), DAI (Fig. 3C), colon length (Fig. 3D and E, Fig. S9A), spleen weight (Fig. S9B and S9C), spleen index (Fig. S9D), pathological evaluation (Fig. 3F) and histological score (Fig. 3G) between the ABX + DSS group and ABX + DSS + **2** group. In addition, we also measured the levels of proinflammatory cytokines and inducible enzymes by RT-qPCR and immunoblotting analysis. Indeed, 5*S*-heudelotinone (**2**) no longer weakened the inflammatory response after gut microbiota depletion (Fig. 3H−M). These results indicate that the protective effect of 5*S*-heudelotinone (**2**) against colitis depends on the gut microbiota.

3.4. 5*S*-Heudelotinone treatment alters the diversity and composition of the gut microbiota

To determine whether 5*S*-heudelotinone (**2**) treatment altered the gut microbiome, high-throughput gene-sequencing analysis of 16S rRNA was performed with fecal bacterial DNA that was isolated from mice in the Control group, DSS group and DSS + **2** group. The number of unique amplicon sequence variants (ASVs) in the DSS group was 11,176, which was significantly lower than that in the Control group (16,506), while the number was dramatically increased after 5*S*-heudelotinone (**2**) treatment, reaching 15,923 (Fig. 4A and Supporting Information Fig. S10). Then, employing a generalized linear model *via* diverse methodologies, we measured the gut microbial alpha diversity. Different indices (including the Chao, observed-species, Shannon and Simpson indices) displayed similar trends. Compared with the Control group, the DSS group showed a prominent decrease in the alpha diversity index. However, 5*S*-heudelotinone (**2**) treatment reversed this trend and resulted in a significantly higher alpha diversity than treatment with DSS alone (Fig. 4B). Next, beta diversity analysis was conducted to generate a principal coordinate analysis (PCoA) plot based on the Jaccard distance, Bray−Curtis metric distance and unweighted UniFrac distance algorithms. An apparent separation cluster among ASVs revealed the different community structures among the three groups, suggesting that these communities were distinct in terms of their compositional structures

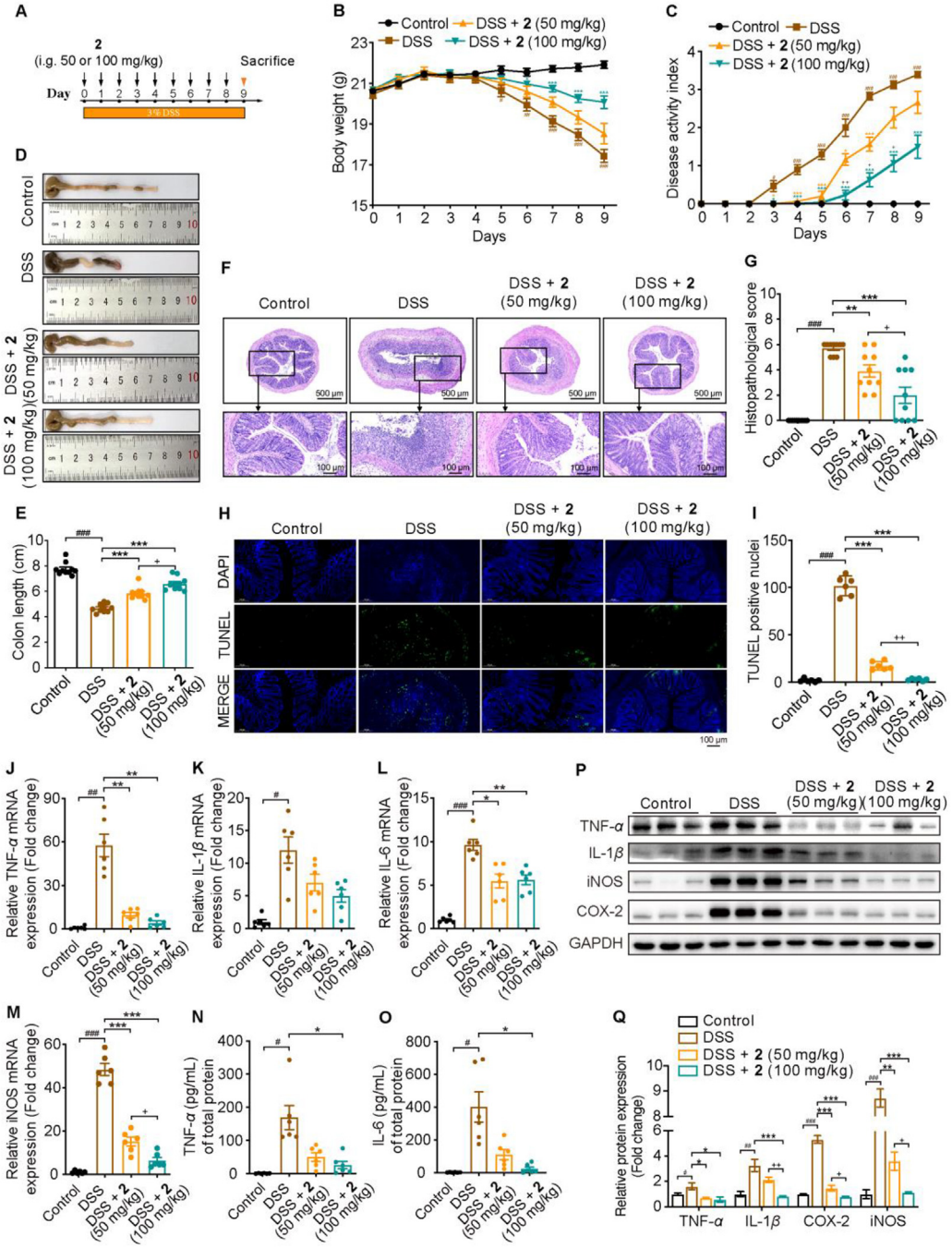

Figure 2 5*S*-Heudelotinone (**2**) treatment preemptively ameliorates DSS-induced colitis. (A) Procedure for establishing a DSS-induced acute colitis model in C57BL/6J mice and 5*S*-heudelotinone (**2**) treatment. (B) Changes in the body weights of mice in the four groups (Control, DSS, 50 mg/kg 5*S*-heudelotinone (**2**) and 100 mg/kg 5*S*-heudelotinone (**2**)). (C) DAI of mice in the four groups. (D, E) Representative images and statistical analysis of colon length of mice in the four different groups on Day 9 ($n = 10$ per group). (F, G) Representative images of H&E staining of histological distal colon sections from the different groups and histological scores ($n = 10$ per group). Scale bars: 500 μm, 100 μm. (H, I) TUNEL assay. TUNEL-positive nuclei, as indicated by fluorescence, represent apoptotic cells. The percentages of apoptotic cells in the distal colon sections are shown in the scatter plot, and representative images of TUNEL-positive cells from each group are shown ($n = 6$ per group). Scale bar: 100 μm. (J−M) The mRNA levels of TNF-α, IL-1β, IL-6 and iNOS in colon tissue from each group were quantified by RT-qPCR ($n = 6$ per group). (N, O) The levels of the cytokines TNF-α and IL-6 in colon tissues from each group were measured by ELISA ($n = 6$ per group). (P) The levels of inflammatory cytokines and inducible enzymes were analyzed by immunoblotting analysis. (Q) Statistical analysis of the expression levels of inflammatory cytokines and inducible enzymes. The data are presented as the mean ± SEM; *P* values are calculated by two-way ANOVA with Turkey's multiple comparisons test (B−C), one-way ANOVA with Dunnett's T3 multiple comparisons test (E, I, J−O) and unpaired two-tailed Student's *t* test (G, Q): $^{\#}P < 0.05$, $^{\#\#}P < 0.01$, $^{\#\#\#}P < 0.001$ (DSS group *vs*. Control group); $^{*}P < 0.05$, $^{**}P < 0.01$, $^{***}P < 0.001$ (5*S*-heudelotinone treatment groups *vs*. DSS group); $^{+}P < 0.05$, $^{++}P < 0.01$ (50 mg/kg 5*S*-heudelotinone group *vs*. 100 mg/kg 5*S*-heudelotinone group).

(Fig. 4C). These results reveal that 5*S*-heudelotinone (**2**) alters the reduction in gut microbiota diversity and the structures of microbial communities in mice that are challenged with DSS.

Subsequently, to further elucidate the bacterial community profiles in the three groups, we assessed the impact of 5*S*-heudelotinone (**2**) on the bacterial composition and relative abundance of the gut microbiota. At the phylum level, each group had almost the same predominant microbial taxa, including *Firmicutes*, *Bacteroidetes*, *Proteobacteria*, *Verrucomicrobia* and *Deferribacteres*, but these taxa were present at different ratios in the different groups (Fig. 4D). *Firmicutes* and *Bacteroidetes* accounted for 49.70% and 47.46% of the intestinal flora in the Control group, respectively. However, the proportion of *Bacteroidetes* was dramatically decreased to 25.46% in the DSS group, while 5*S*-heudelotinone (**2**) reversed this effect, increasing the abundance of *Bacteroidetes* up to 53.29% (Fig. 4E). Additionally, the phyla *Proteobacteria* and *Deferribacteres* were present in relatively high abundances in the DSS group (10.76% and 1.11%, respectively), whereas their abundances were significantly decreased to 1.76% and 0.10% in the DSS + **2** group (Fig. 4F and G). Moreover, the *Firmicutes* to *Bacteroidetes* ratio (F/B) was altered by DSS treatment, which is typically observed in IBD. After treatment with 5*S*-heudelotinone (**2**), the ratio was restored to normal levels (Fig. 4H). Taxonomic compositions were also compared at the class/order/family levels (Supporting Information Fig. S11). Notably, at the genus level, the abundances of S24-7 and *Odoribacter* were dramatically decreased in the DSS group but enriched in the 5*S*-heudelotinone (**2**)-treated group (Fig. 4J and K). Among these genera, *Odoribacter* is a genus of butyrate-producing bacteria with anti-inflammatory properties that alleviates IBD, and S24-7 is a clade that is associated with treatment-induced remission of murine colitis. Moreover, 5*S*-heudelotinone (**2**) also increased the percentage of *Akkermansia*, which has been proposed to act as a potential probiotic (Supporting Information Fig. S12A). Moreover, the relative abundances of *Shigella*, *Parabacteroides* and *Clostridium*, which are virulent pathogens that have been reported to promote IBD, were significantly reduced after 5*S*-heudelotinone (**2**) treatment (Fig. 4L, Fig. S12B and S12C). These results indicate that 5*S*-heudelotinone (**2**) could dramatically increase the proportion of beneficial bacteria and decrease the abundance of pathogenic bacteria.

Next, high-dimensional class comparisons were performed to identify marked differences in the predominant bacterial communities between the DSS group and 5*S*-heudelotinone (**2**)-treated group *via* linear discriminant analysis (LDA) of effect size (LEfSe). As a result, the genus *Lactobacillus* (from the class *Bacilli* to the family *Lactobacillaceae*) and the genus *Shigella* (from the class *Gammaproteobacteria* to the family *Enterobacteriaceae*) were the key strains that caused dysbiosis of the gut microbiota in the DSS group. Nevertheless, the family S24-7 (from the phylum *Bacteroidetes* to the order *Bacteroidales*), the genus *Odoribacter* (from the phylum *Bacteroidetes* to the family *Odoribacteraceae*), and the genus *Butyricicoccus* were enriched in the 5*S*-heudelotinone (**2**)-treated group, which might be associated with the effect of 5*S*-heudelotinone (**2**) on ameliorating colitis (Fig. 4M). Furthermore, we organized a comparison cladogram and heatmap to analyze the gut microbiota in the two groups (Fig. 4N). In conclusion, treatment with 5*S*-heudelotinone (**2**) strikingly alters the diversity and composition of the gut microbiota.

3.5. 5*S*-Heudelotinone treatment increases metabolite SCFAs

The gut microbiota contributes to the production of various metabolites; thus, changes in the composition and abundance of gut microbes always lead to changes in microbial metabolites. Since we found that SCFA-producing bacteria were predominant in the 5*S*-heudelotinone (**2**)-treated group, we explored the effect of 5*S*-heudelotinone (**2**) on SCFAs, a kind of microbial metabolites that play key roles in maintaining intestinal homeostasis. Targeted metabolomics was used to evaluate the concentration of SCFAs in fecal samples. As shown in Fig. 5, the concentrations of butyric acid and valeric acid in the feces from mice in the DSS group were significantly reduced compared to those in the feces from mice in the Control group (Fig. 5C and E). After 5*S*-heudelotinone (**2**) administration, the levels of seven SCFAs tended to increase, with significant differences observed in the levels of propionic acid, butyric acid, isobutyric acid and valeric acid compared with those in the DSS group (Fig. 5B−E); however, there were no statistically significant differences in the levels of acetic acid, isobutyric acid and caproic acid (Fig. 5A−F and G). Next, Spearman's rank correlation analysis was performed to investigate the relationship between the microbial community and SCFAs. At the phylum level, the relative abundance of *Proteobacteria* and *Deferribacteres* was negatively correlated with the levels of propionic acid, butyric acid and valeric acid, and the level of *Verrucomicrobia* was positively correlated with the levels of isobutyric acid and valeric acid (Fig. 5H). At the genus level, S24-7 and *Ruminnococcus* exhibited positive correlations with propionic acid, butyric acid and valeric acid; *Akkermansia* showed positive correlations with isobutyric acid and valeric acid; and *Parabacteroides*, *Prevotella*, *Sutterella*, *Enterococcus* and *Mucispirillum* were negatively correlated with propionic acid, butyric acid and valeric acid (Fig. 5I). In summary, these results suggest that treatment with 5*S*-heudelotinone (**2**) can increase the concentrations of SCFAs in feces, especially the concentrations of butyric acid and valeric acid, which is consistent with the finding that SCFA-producing bacteria are the predominant bacteria in the 5*S*-heudelotinone (**2**)-treated group.

3.6. 5*S*-Heudelotinone shapes intestinal immune responses by regulating both innate and adaptive immune signaling in a gut microbiota-dependent manner

The crosstalk between the gut microbiota and immune system is complex and is partially dependent on microbial metabolites, such as SCFAs. SCFAs, especially butyric acid, perform important immunomodulatory functions, including the regulation of both innate and adaptive cells[16]. Considering that 5*S*-heudelotinone (**2**) affected the concentration of SCFAs, we next explored whether 5*S*-heudelotinone (**2**) affects intestinal mucosal immunity. First, we examined the infiltration of innate immune cell populations in the colon *via* flow cytometry. Consistent with previous studies, the proportions of macrophages, DCs and MDSCs in the intestinal tissues dramatically increased with the development of colitis. Interestingly, treatment with 5*S*-heudelotinone (**2**) at both dosages (50 and 100 mg/kg) significantly reduced the numbers of these three types of immune cells (Fig. 6A). Given that the spleen is the largest immune organ in the body, its abnormal enlargement might reflect immune system disorder. Therefore, we also analyzed the proportions of macrophages and DCs in the spleen tissues of mice. Consistent with the changes in colon tissue, the numbers of these

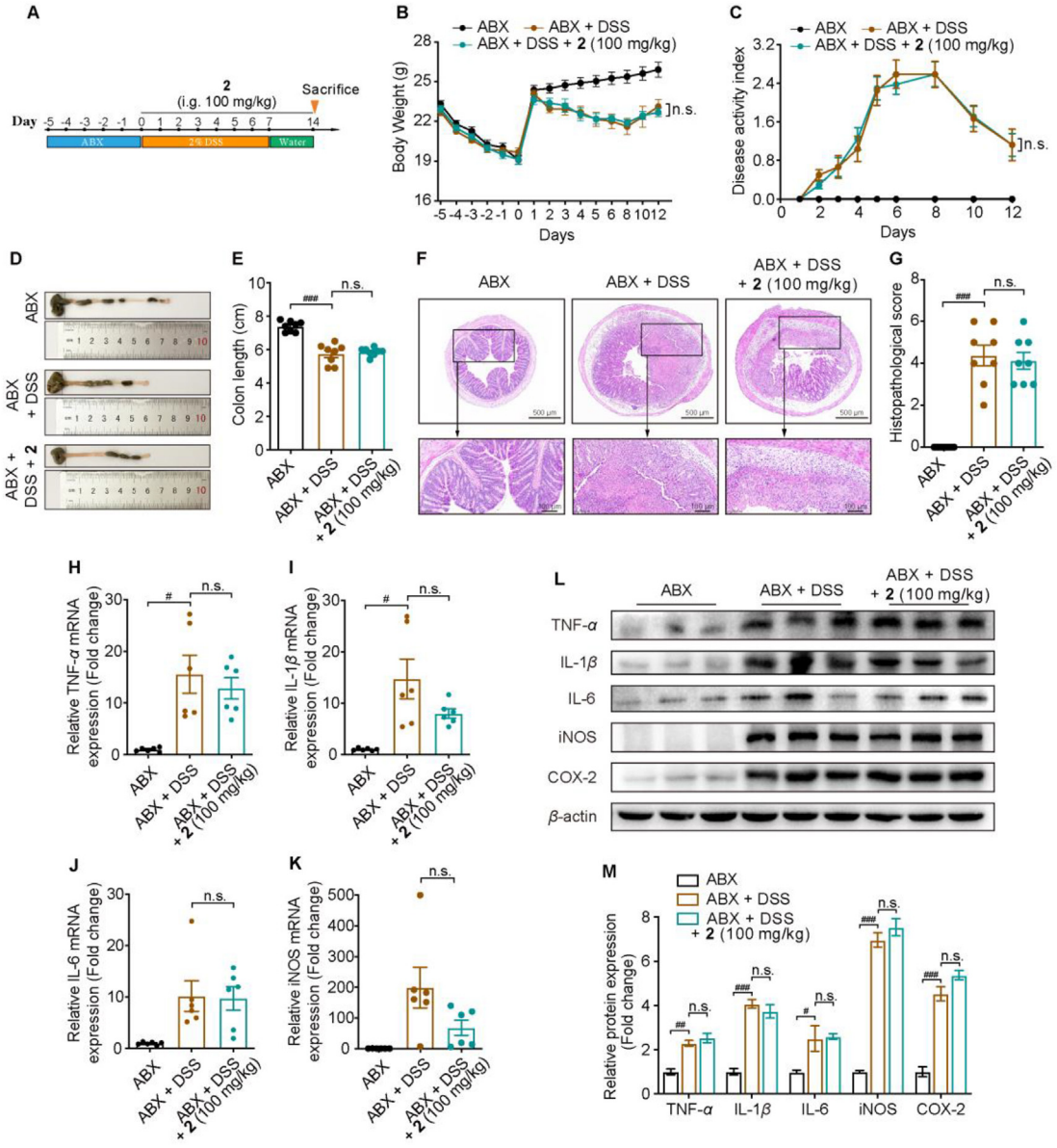

Figure 3 5*S*-Heudelotinone (**2**) attenuates DSS-induced colitis in a gut microbiota-dependent manner. (A) Procedure for establishing a gut microbiota-depleted model in C57BL/6J mice and 5*S*-heudelotinone (**2**) treatment. (B) Changes in the body weights of mice in the three groups (ABX, ABX + DSS, ABX + DSS + **2**). (C) DAI of mice in the three groups. (D, E) Representative images and statistical histogram of colons from the different groups on Day 14 ($n = 8$ per group). (F, G) Representative images of H&E staining of histological distal colon sections from the different groups and histological scores ($n = 8$ per group). Scale bars: 500 μm, 100 μm. (H−K) The mRNA levels of TNF-α, IL-1β, IL-6 and iNOS in colon tissues from each group were quantified by RT-qPCR ($n = 6$ per group). (L) The levels of inflammatory cytokines and inducible enzymes were analyzed by immunoblotting analysis. (M) Statistical analysis of the expression levels of inflammatory cytokines and inducible enzymes. The data are presented as the mean ± SEM; *P* values are calculated by two-way ANOVA with Turkey's multiple comparisons test (B−C), one-way ANOVA with Dunnett's T3 multiple comparisons test (E, H−K) and unpaired two-tailed Student's *t* test (G, M): $^{\#}P < 0.05$, $^{\#\#}P < 0.01$, $^{\#\#\#}P < 0.001$ (ABX group *vs.* ABX + DSS group); n.s. = not significant.

two types of immune cells in the spleens of DSS-induced colitis mice were decreases by 5*S*-heudelotinone (**2**) treatment (Supporting Information Fig. S13A). Collectively, these findings suggest that 5*S*-heudelotinone (**2**) treatment leads to a decrease in the numbers of innate immune cells, including macrophages, DCs and MDSCs.

In addition, adaptive immune disorders, including imbalances in Th17 and Treg cells, are believed to be the fundamental cause of IBD. To investigate the impact of 5*S*-heudelotinone (**2**) on Th17 and Treg cells, flow cytometry was used to analyze T-cell response phenotypes in both colon and spleen tissues. Compared with the Control group, an increased proportion of IL-17A-expressing $CD4^+$ T cells (Th17) was observed in the colons of DSS-treated mice, and 5*S*-heudelotinone (**2**) treatment reversed this effect at both dosages (Fig. 6B). Considering that Th17 cells are a major source of proinflammatory cytokine IL-17A secretion, this result

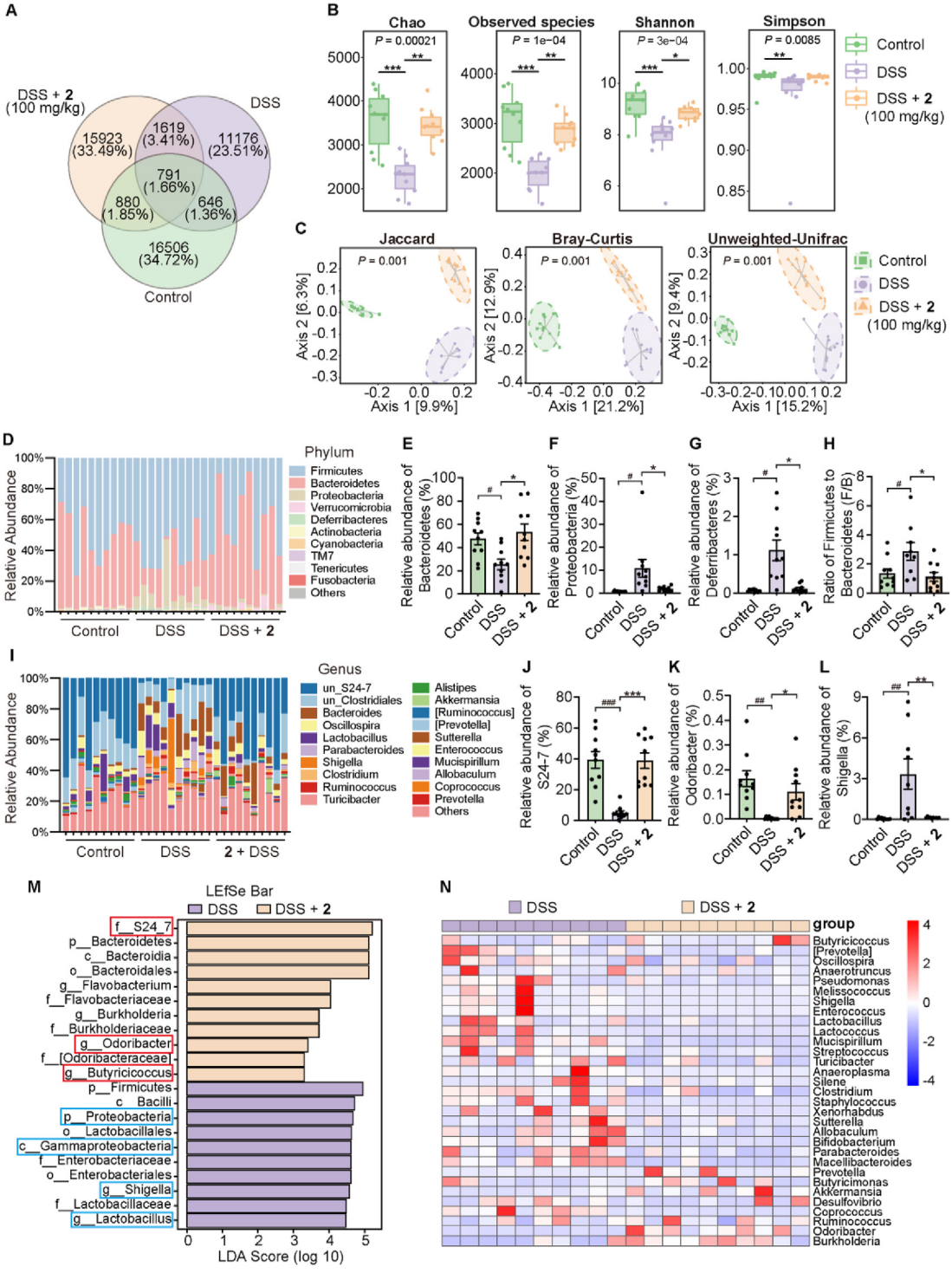

Figure 4 5*S*-Heudelotinone (**2**) treatment significantly alters the diversity and composition of the gut microbiota. (A) Venn diagram of ASVs of the gut microbiota in mice from each group. (B) Alpha diversity boxplot (including the Chao, observed species, Shannon and Simpson indices). (C) Genus-level PCoA plot based on Jaccard, Bray−Curtis metric and unweighted UniFrac distance algorithms. (D) Bar plots of the phylum taxonomic levels in the Control, DSS and DSS + **2** groups. (E) Relative abundance of *Bacteroidetes* in the three groups. (F) Relative abundance of *Proteobacteria* in the three groups. (G) Relative abundance of *Deferribacteres* in the three groups. (H) *Firmicutes* to *Bacteroidetes* ratio (F/B) in the three groups. (I) Bar plots of the genus taxonomic levels in the Control, DSS and DSS + **2** groups. (J) Relative abundance of S24-7 in the three groups. (K) Relative abundance of *Odoribacter* in the three groups. (L) Relative abundance of *Shigella* in the three groups. (M) LDA score plot of differentially abundant taxonomic features between the DSS group and DSS + **2** group (the criterion for feature selection is log LDA score >3). (N) Heatmap of the 30 most differentially abundant taxa between the DSS group and DSS + **2** group at the genus level. $n = 10$. The data are presented as the mean ± SEM; *P* values are calculated by one-way ANOVA with Dunnett's T3 multiple comparisons test: $^{\#}P < 0.05$, $^{\#\#}P < 0.01$, $^{\#\#\#}P < 0.001$ (DSS group *vs.* Control group); $^{*}P < 0.05$, $^{**}P < 0.01$, $^{***}P < 0.001$ (5*S*-heudelotinone treatment groups *vs.* DSS group).

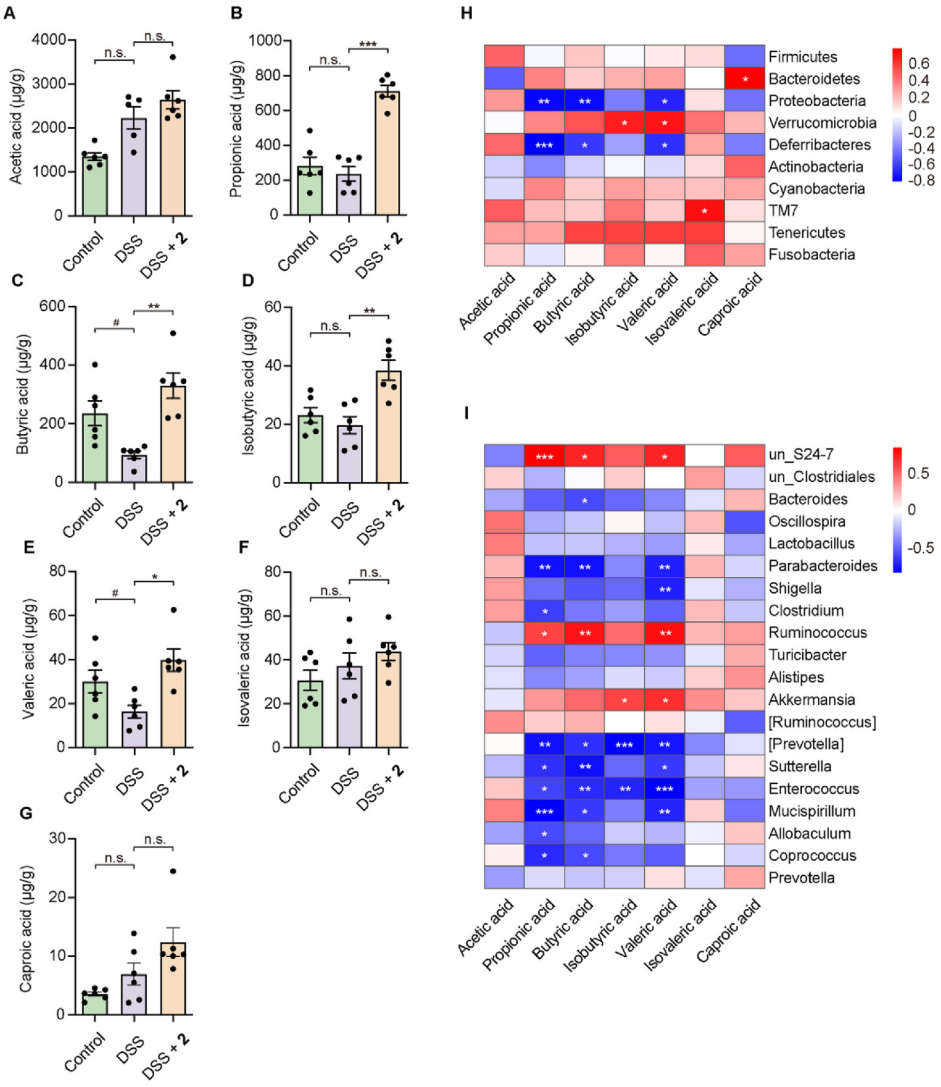

Figure 5 5*S*-Heudelotinone (**2**) treatment increases the concentrations of microbial metabolite SCFAs. Concentrations of (A) acetic acid, (B) propionic acid, (C) butyric acid, (D) isobutyric acid, (E) valeric acid, (F) isovaleric acid and (G) caproic acid in the feces from mice in the three groups. Heatmap of the Spearman correlation between SCFA levels and the gut microbiota at the (H) phylum level and (I) genus level in the DSS and DSS + **2** groups. Positive correlations are represented in red, and negative correlations are represented in blue. $n = 6$. The data are presented as the mean ± SEM; *P* values are calculated by one-way ANOVA with Dunnett's T3 multiple comparisons test: $^{\#}P < 0.05$ (DSS group *vs.* Control group); $^{*}P < 0.05$, $^{**}P < 0.01$, $^{***}P < 0.001$ (5*S*-heudelotinone treatment group *vs.* DSS group); n.s. = not significant.

indicated that 5*S*-heudelotinone (**2**) may inhibit the production of IL-17A by reducing the proportion of Th17 cells. Moreover, we found that the percentage of Treg cells was increased in the colons of DSS-treated mice, and 5*S*-heudelotinone (**2**) restored the proportion of Treg cells to the level that was observed in the Control group (Supporting Information Fig. S14). This result might have occurred due to the abnormal increase in Th17 cell numbers, which may have led to a compensatory increase in Treg cell numbers. Similarly, we also measured the proportions of Th17 and Treg cells in the spleen tissues of mice. Compared with the Control group, the ratio of Th17 cells was significantly increased and the ratio of Treg cells was dramatically decreased in the DSS group, but both dosages of 5*S*-heudelotinone (**2**) reversed these effects (Fig. S13B).

To further investigate whether the 5*S*-heudelotinone (**2**)-induced changes in immune cells depend on the gut microbiota, immune cells were isolated from the colon tissues of gut microbiota-depleted mice and analyzed by flow cytometry. The percentages of macrophages, DCs and MDSCs were not significantly different between the ABX + DSS group and the ABX + DSS + 5*S*-heudelotinone (**2**) group (Fig. 6C). Consistent with this finding, the number of Th17 and Treg cells exhibited corresponding changes in the gut microbiota depletion groups (Fig. 6D and Supporting Information Fig. S15). We also analyzed the proportions of these immune cells in spleen tissues. The results showed that the ABX + DSS + 5*S*-heudelotinone (**2**) group displayed a trend that was similar to that in the ABX + DSS group after the gut microbiota was depleted (Supporting Information Fig. S16). These results indicate that the 5*S*-heudelotinone (**2**)-induced changes in the gut microbiota are responsible for the inhibition of innate immune cells and the decrease in the proportion of Th17 cells, which thereby relieve the symptoms of

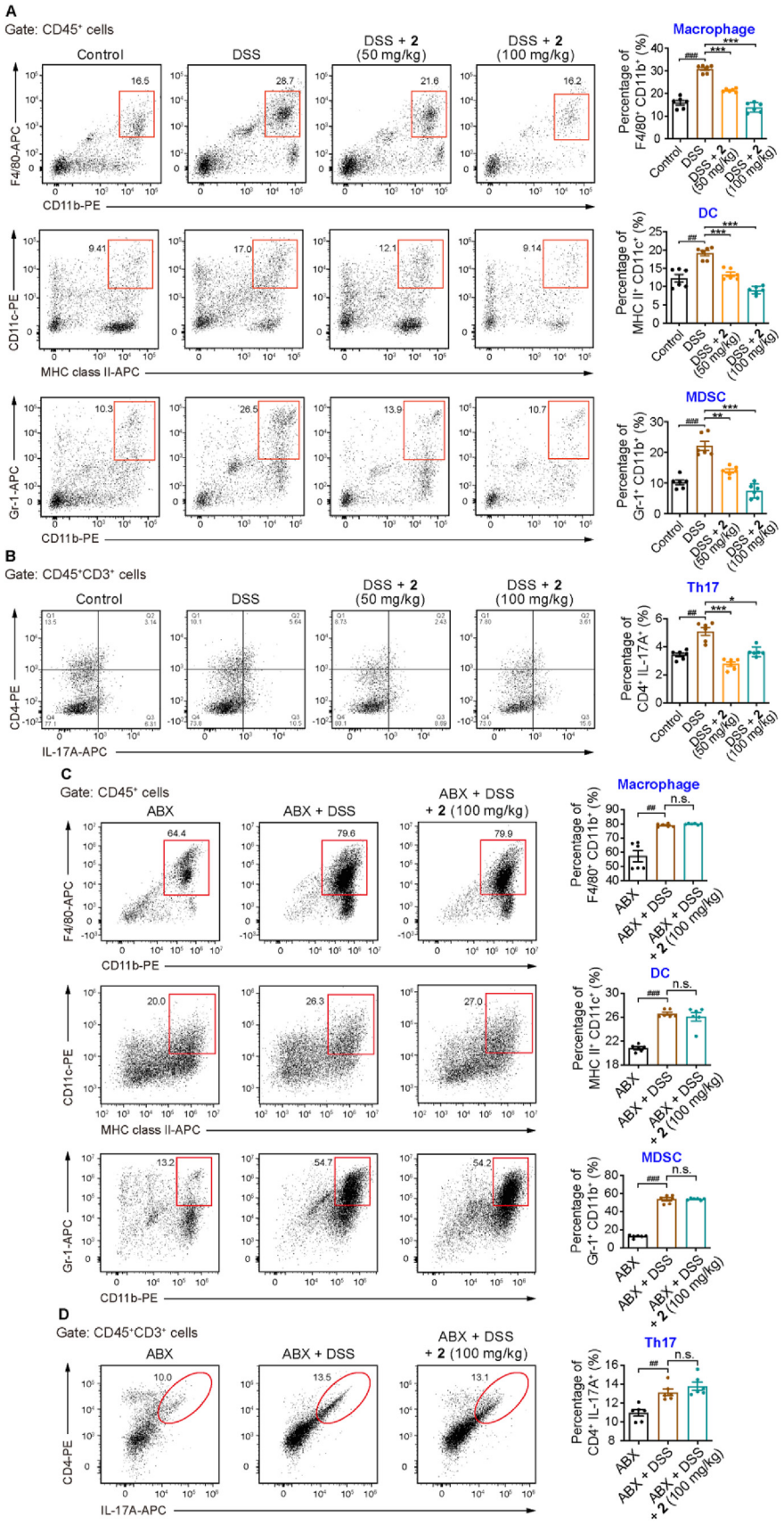

Figure 6 5*S*-Heudelotinone (**2**) treatment regulates the proportion of innate immune cells and Th17 cells in a gut microbiota-dependent manner. (A) Representative staining and percentages of macrophages (F4/80$^+$ CD11b$^+$), DCs (major histocompatibility complex (MHC) class II$^+$ CD11c$^+$) and MDSCs (Gr-1$^+$ CD11b$^+$) among CD45$^+$ cells from colon tissues of each group. $n = 6$. Dot plots are gated on CD45$^+$ cells. Numbers adjacent to the outlined areas indicate the percentage of the gated population in each group. (B) Representative staining and percentage

colitis. In other words, 5*S*-heudelotinone (**2**) regulates the immune system in a gut microbiota-dependent manner.

3.7. 5S-Heudelotinone enhances intestinal barrier integrity in a gut microbiota-dependent manner

The intestinal barrier bridges the gap between the gut microbiota and the intestinal immune system and thus maintains mucosal homeostasis[58]. Moreover, it is well established that SCFAs, particularly butyric acid, are important for promoting epithelial barrier function and maintaining the intestinal barrier integrity [17]. Therefore, we suggest that 5*S*-heudelotinone (**2**) also affects the continuous intercellular barrier, especially TJs. Consequently, the expression levels of TJ proteins, including Claudins, ZO-1 and Occludin, were examined by RT-qPCR. The mRNA level of Claudin-2 was significantly increased in the mice with colitis, and the levels of Claudin-4, Claudin-7, Occludin and ZO-1 were dramatically downregulated; these results were consistent with previous reports on mice with colitis. Notably, 5*S*-heudelotinone (**2**) treatment reversed these trends in TJ protein expression in mice with colitis to some extent (Fig. 7A−E). Next, we verified the protein levels of TJ Proteins, including Claudin-2, Claudin-4, Claudin-7, ZO-1 and Occludin, by western blotting. The results showed that 5*S*-heudelotinone (**2**) treatment significantly ameliorated the changes in TJ protein expression caused by DSS (Fig. 7F and G). To visualize the expression level and localization of ZO-1 and Occludin, immunofluorescence staining was performed. Both TJ proteins were present along the inner lining of the columnar epithelium of the colon, and the expression levels were dramatically decreased in mice with colitis but increased after treatment with 5*S*-heudelotinone (**2**) (Fig. 7H and I). These results indicate that 5*S*-heudelotinone (**2**) restores the expression of TJ proteins and therefore maintains the barrier function of the intestinal epithelium. Additionally, we examined the expression levels of these TJ proteins in a DSS-induced colitis model after gut microbiota depletion and treatment with or without 5*S*-heudelotinone (**2**) by RT-qPCR and immunoblotting analysis. The results showed that the changes in the expression of these TJ proteins were consistent with the findings in the colitis model mice described above, but treatment with 5*S*-heudelotinone (**2**) could no longer reverse the effects of DSS when the gut microbiota was depleted (Fig. 7J−P). In summary, the gut microbiota plays a crucial role in the enhancement of intestinal barrier integrity by 5*S*-heudelotinone (**2**).

3.8. 5S-Heudelotinone alleviates the ongoing colitis

To further determine whether 5*S*-heudelotinone (**2**) can alleviate ongoing colitis, we adjusted the experimental procedure. That is, we first established the DSS-induced colitis model, and then, when most mice exhibited decreased body weight and diarrhea, we therapeutically treated these mice with 5*S*-heudelotinone (**2**) (Fig. 8A). Compared with mice in the Control group, a successive 7-day administration of DSS resulted in significant weight loss and bloody stool in the other three groups of mice. Among these groups of mice, mice in two groups were administered 5*S*-heudelotinone (**2**) at dosages of 50 and 100 mg/kg once per day, and the other group was administered solvent. After therapeutic treatment for 7 days, 5*S*-heudelotinone (**2**) attenuated the clinical symptoms of colitis, including the severe weight loss (Fig. 8B), higher DAI (Fig. 8C), shortened colon length (Fig. 8D and E, Supporting Information Fig. S17A), splenomegaly (Fig. S17B−S17D) and abnormal pathology (Fig. 8F and G); these results indicated that both dosages of 5*S*-heudelotinone (**2**) exerted profound therapeutic effects on ameliorating the symptoms of colitis, and there was no marked difference between low-dose and high-dose 5*S*-heudelotinone (**2**). In addition, TUNEL staining was also performed on colon tissues from mice of each group. Compared with the Control group, the number of TUNEL-positive nuclei was significantly increased in the DSS group, while this number was sharply decreased in both the 5*S*-heudelotinone (**2**)-treated groups, indicating that 5*S*-heudelotinone (**2**) could prevent apoptosis in colon tissues, thereby alleviating DSS-induced intestinal mucosal damage and restoring intestinal barrier integrity (Fig. 8H and I). These results show that 5*S*-heudelotinone (**2**) also provides therapeutic benefits against DSS-induced colitis in mice.

3.9. 5S-Heudelotinone reduces CAC development in mice

IBD is an independent risk factor for the occurrence and development of CAC[3]. To verify whether 5*S*-heudelotinone (**2**) affects the development of CAC, we combined the procarcinogen AOM with 3 cycles of 2% DSS to chemically trigger CAC; then, the mice were treated with 5*S*-heudelotinone (**2**) daily in parallel with the AOM/DSS protocol (Fig. 9A). First, we evaluated the weight of the mice to assess disease development. The results showed that in the first round of DSS administration, the mice in the three model groups all exhibited weight loss. Beginning on the 4th day, the weights of mice in the AOM (AOM/DSS-treated only) group significantly declined and reached the lowest value on the second day after the resumption of normal drinking water. Compared with the AOM group, the weights of mice in the two 5*S*-heudelotinone (**2**)-treated groups began to decrease until the 6th day, and diarrhea and hematochezia were greatly ameliorated compared with those in the AOM group. After two weeks of recovery, the symptoms and physical signs of the mice in the three groups steadily recovered. In the remaining two rounds of DSS treatment, the colitis-induced morbidity was similar to that in the first round even

of Th17 cells ($CD4^+$ $IL\text{-}17A^+$) among $CD45^+$ $CD3^+$ cells from colon tissues of each group. $n = 6$. Dot plots are gated on $CD45^+$ $CD3^+$ cells. Numbers adjacent to the outlined areas indicate the percentage of the gated population in each group. (A, B) The data are presented as the mean ± SEM; *P* values are calculated by one-way ANOVA with Dunnett's T3 multiple comparisons test: $^{\#\#}P < 0.01$, $^{\#\#\#}P < 0.001$ (DSS group *vs*. Control group); $^{*}P < 0.05$, $^{**}P < 0.01$, $^{***}P < 0.001$ (5*S*-heudelotinone treatment groups *vs*. DSS group). (C) Representative staining and percentages of macrophages ($F4/80^+$ $CD11b^+$), DCs (MHC class II^+ $CD11c^+$) and MDSCs ($Gr\text{-}1^+$ $CD11b^+$) among $CD45^+$ cells from colon tissues of the gut microbiota depletion groups. $n = 6$. Dot plots are gated on $CD45^+$ cells. Numbers adjacent to the outlined areas indicate the percentage of the gated population in each group. (D) Representative staining and percentages of Th17 cells ($CD4^+$ $IL\text{-}17A^+$) among $CD45^+$ $CD3^+$ cells from colon tissues of the gut microbiota depletion groups. $n = 6$. Dot plots are gated on $CD45^+$ $CD3^+$ cells. Numbers adjacent to the outlined areas indicate the percentage of the gated population in each group. (C, D) The data are presented as the mean ± SEM; *P* values are calculated by one-way ANOVA with Dunnett's T3 multiple comparisons test: $^{\#\#}P < 0.01$, $^{\#\#\#}P < 0.001$ (ABX + DSS group *vs*. ABX group); n.s. = not significant.

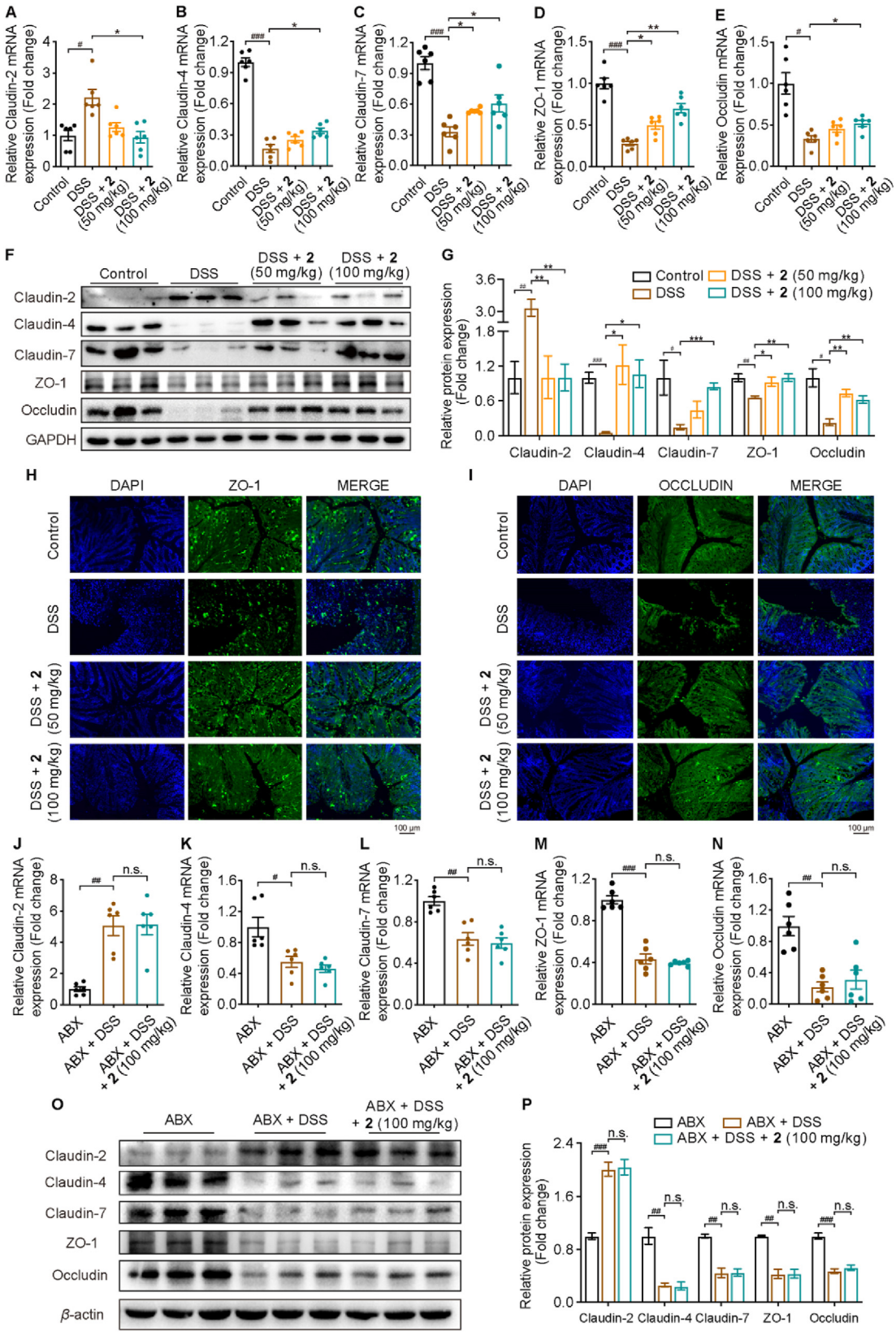

Figure 7 The protective effect of 5*S*-heudelotinone (**2**) against TJ disruption is dependent on the gut microbiota. (A−E) The mRNA levels of Claudin-2, Claudin-4, Claudin-7, ZO-1 and Occludin in colon tissues from each group were quantified by RT-qPCR. (F) The TJ protein levels of Claudin-2, Claudin-4, Claudin-7, ZO-1 and Occludin in colon tissues from each group were assessed by immunoblotting analysis. (G) Statistical analysis of TJ protein expression levels. (H, I) The localization and expression levels of ZO-1 and Occludin were determined by immunofluorescence staining. Scale bar: 100 μm. (A−G) The data are presented as the mean ± SEM; *P* values are calculated by one-way ANOVA with

though the symptoms were quite different: the mice in the AOM group presented mild symptoms in the second round of DSS treatment but severe weight loss and hematochezia in the third round because of the different stages of colitis and tumor occurrence and development (Fig. 9B). Consistent with the effects on DSS-induced colitis, 5*S*-heudelotinone (**2**) treatment also increased colon and intestine lengths (Fig. 9C and Supporting Information Fig. S18A and S18B). Moreover, at the end of the 12th week, 100% of mice in the AOM group developed tumors throughout the entire colon, especially in the middle to distal portion (Fig. 9D). However, only 62.5% of the mice in the low-dose group and 32.5% of the mice in the high-dose group showed tumor formation (Fig. 9E). Furthermore, 5*S*-heudelotinone (**2**) treatment significantly decreased the number of tumors per mouse and reduced the average size of the tumors compared with AOM alone. As shown in Fig. 9F, the tumor size of the mice in the AOM group (diameters of $\geq$3 mm) was generally larger than that of the mice in the 5*S*-heudelotinone (**2**)-treated groups (diameters of 1−2 mm). In addition, mice in the AOM group exhibited higher tumor loads in their small intestines, with 7.1 adenomas per mouse, whereas mice in the low-dose and high-dose 5*S*-heudelotinone (**2**) groups developed an average of 4.2 and 4.1 adenomas per mouse, respectively (Fig. S18C). We also measured the weights of the spleens from mice in the different groups. The results showed that the spleen weight of the mice in the high-dose group returned to the level observed in the Control group when the mice were treated with 5*S*-heudelotinone (**2**) (Fig. S18D and S18E). Finally, the colonic tissues were prepared as Swiss rolls and processed for H&E and Ki67 staining. Histological examinations demonstrated that the colon tissue structures of mice in the AOM group was disordered, as evidenced by disrupted crypt architecture and goblet cells, thickened and fibrotic muscle layers, distorted gland structures, enlarged and darkly stained nuclei, large adenomas in the middle and distal portion of colon and abundant inflammatory cell infiltration. In contrast, in both 5*S*-heudelotinone (**2**)-treated groups, the colon tissue mucosa was relatively complete, the crypt architecture and goblet cells were only slightly disrupted, and the infiltration of inflammatory cells was decreased. Moreover, hyperplasia was decreased and mostly located in the distal portion of the intestine, and the degree of tumor malignancy was significantly lower than that in the AOM group (Fig. 9G). In addition, Ki67 staining showed that 5*S*-heudelotinone (**2**) treatment markedly decreased the numbers of Ki67-positive cells, indicating that the number of malignant proliferating cells and degree of tumor malignancy were both reduced (Fig. 9H). These results demonstrate that 5*S*-heudelotinone (**2**) potently reduces CAC development in mice.

4. Discussion

IBD is a set of chronic inflammatory conditions that affect the GI tract, and it occurs in patients worldwide; however, no effective and safe therapies have been developed for use in clinic[1,5]. Changing the composition of the gut microbiota and related metabolites have been proposed as novel approaches for treating autoimmune diseases, including IBD[10]. In this research, we initially synthesized the racemate of heudelotinone and investigated the protective and therapeutic role of 5*S*-heudelotinone (**2**) (one of the enantiomers) on DSS-induced colitis, as evidenced by the reversal of body weight loss, DAI, shortened colon length and histology score. Importantly, the beneficial effects of 5*S*-heudelotinone (**2**) depended on the gut microbiota, as shown by the finding that these effects were lost in an ABX-treated mouse model. Analysis of 16S rRNA gene sequencing and targeted metabolomics revealed that 5*S*-heudelotinone (**2**) enriched the abundance and diversity of the gut microbiota, increased the proportion of SCFA-producing bacteria as well as the production of SCFAs, and decreased the ratio of pathogenic bacteria. *Via* an upregulation in SCFA levels, 5*S*-heudelotinone (**2**) sequentially modulated the intestinal immune system and promoted the intestinal mucosa integrity. Notably, these protective effects were abrogated by the administration of ABX prior to the induction of colitis, providing further verification that the effect of 5*S*-heudelotinone (**2**) depends on the gut microbiota (Fig. 10).

Icetexanes are natural diterpenoid products that are characterized by a [6,7,6]-tricyclic core that is supposed to be constructed *via* the rearrangement of [6,6,6]-fused abietane diterpenoids[59]. Diterpenoids have been reported to have various biological activities, including anticancer, antibacterial and anti-inflammatory activities[60,61]. Importantly, diterpenoids have been identified as potential therapeutic agents for treating IBD; however, the precise molecular mechanisms underlying their effects remain elusive, and only a limited number of candidates have advanced to clinical trials. Therefore, exploring the pharmacological activity of diterpenoids against IBD and the underlying mechanism is of great value. Heudelotinone, an icetexane type of dinorditerpenoid, was first isolated from the stem bark and roots of *R. heudelotii* in 1991 and displays antitumor activity and inhibitory activity against thioredoxin reductase (TrxR) *in vitro*[47,52,53]. To verify the exact pharmacological activity and explore the potential clinical value of heudelotinone, we developed a concise and accessible synthetic route to produce ample quantities of heudelotinone for its comprehensive biological evaluation in various animal models. By performing a DA reaction, we rapidly constructed the critical 6-7-6-tricyclic core of heudelotinone. After reduction, elimination and demethylation reactions, compound **12** was ultimately obtained. This efficient synthetic route yielded a racemate of heudelotinone on a gram scale through only 6 linear steps starting from known compound **6**, with an overall yield of 22%. A pair of enantiomers, namely, 5*R*-heudelotinone (**1**) and 5*S*-heudelotinone (**2**), were obtained by chiral separation *via* chiral HPLC, and their absolute configurations were determined by X-ray diffraction of single crystals. Considering the traditional anti-inflammatory activity of diterpenoids, we explored the effects of 5*R*-heudelotinone (**1**) and 5*S*-heudelotinone (**2**) on experimental colitis. Notably, 5*S*-heudelotinone (**2**) exerted a

Dunnett's T3 multiple comparisons test (A−E) and unpaired two-tailed Student's *t* test (G): $^{\#}P < 0.05$, $^{\#\#}P < 0.01$, $^{\#\#\#}P < 0.001$ (DSS group *vs*. Control group); $^{*}P < 0.05$, $^{**}P < 0.01$, $^{***}P < 0.001$ (5*S*-heudelotinone treatment groups *vs*. DSS group). (J−N) The mRNA levels of Claudin-2, Claudin-4, Claudin-7, ZO-1 and Occludin in colon tissues from the gut microbiota depletion groups were quantified by RT-qPCR. (O) The TJ protein levels of Claudin-2, Claudin-4, Claudin-7, ZO-1 and Occludin in colon tissues from the gut microbiota depletion groups were assessed by immunoblotting analysis. (P) Statistical analysis of TJ protein expression levels. (J−P) The data are presented as the mean ± SEM; *P* values are calculated by one-way ANOVA with Dunnett's T3 multiple comparisons test (J−N) and unpaired two-tailed Student's *t* test (P): $^{\#}P < 0.05$, $^{\#\#}P < 0.01$, $^{\#\#\#}P < 0.001$ (ABX + DSS group *vs*. ABX group); n.s. = not significant.

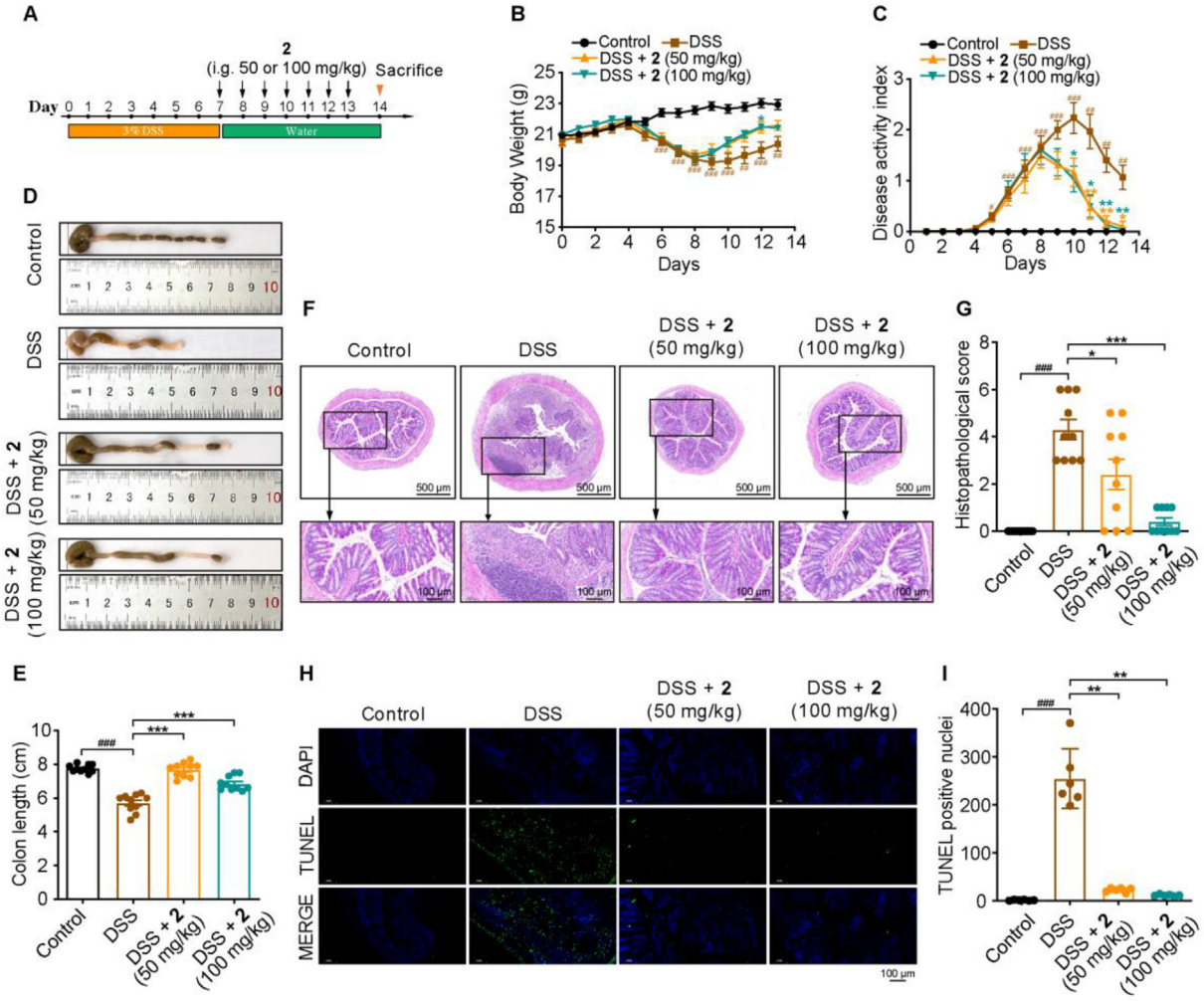

Figure 8 Therapeutic treatment with 5*S*-heudelotinone (**2**) alleviates DSS-induced colitis. (A) Procedure for the therapeutic treatment of DSS-induced acute colitis with 5*S*-heudelotinone (**2**). (B) Changes in the body weights of mice in the four groups (Control, DSS, 50 mg/kg 5*S*-heudelotinone (**2**) and 100 mg/kg 5*S*-heudelotinone (**2**)). (C) DAI of mice in the four groups. (D, E) Representative images and statistical analysis of colon length of mice in the four different groups on day 14 ($n = 10$ per group). (F, G) Representative images of H&E staining of histological distal colon sections and histological scores of different groups ($n = 10$ per group). Scale bars: 500 μm, 100 μm. (H, I) Representative image of TUNEL staining and statistical analysis of TUNEL-positive nuclei ($n = 6$ per group). Scale bar: 100 μm. The data are presented as the mean ± SEM; *P* values are calculated by two-way ANOVA with Turkey's multiple comparisons test (B−C), one-way ANOVA with Dunnett's T3 multiple comparisons test (E, I) and unpaired two-tailed Student's *t* test (G): $^{\#}P < 0.05$, $^{\#\#}P < 0.01$, $^{\#\#\#}P < 0.001$ (DSS group *vs*. Control group); $^{*}P < 0.05$, $^{**}P < 0.01$, $^{***}P < 0.001$ (5*S*-heudelotinone treatment groups *vs*. DSS group).

dramatic effect on IBD and CAC. Importantly, this is the first C_{18} dinorditerpenoid to be studied in the context of experimental IBD, and this study has significant implications for future discovery in the field of natural products.

The human microbiota comprises approximately 1150 bacterial species, and more than 99% of these bacteria belong to the phyla *Firmicutes*, *Bacteroidetes*, *Proteobacteria*, *Verrucomicrobia* and *Deferribacteres*. Recently, the commensal gut microbiota has been found to be both ecologically and functionally disrupted during IBD[11,62]. Common microbial profiles in IBD samples include reduced richness and diversity of the microbiota, decreased relative abundances of *Bacteroidetes* and *Lachnospiraceae*, and increased abundance of *Proteobacteria* and *Actinobacteria*[63,64]. Previous studies have shown that the biodiversity of the fecal microbiota from IBD patients is significantly reduced and that the gut microbiota of IBD patients is unstable compared to that of healthy individuals[65]. In our research, 5*S*-heudelotinone (**2**) dramatically increased the abundance and diversity of the intestinal microbiota in mice with DSS-induced colitis. In addition, multiple studies have investigated differences in the composition of the gut microbiota in IBD patients and healthy individuals. *Proteobacteria* species have been identified as the primary pathogenic bacteria that produce endotoxins, and some members of *Proteobacteria* might be able to exploit host defenses and promote proinflammatory responses in susceptible hosts; thus, the expansion of *Proteobacteria* is thought to be correlated with the inflammatory response to DSS. Moreover, microbial diversity studies have consistently demonstrated an increase in the abundance of *Proteobacteria* in patients with IBD. Notably, the causative agent *Shigella* (from the phylum *Proteobacteria* to the family *Enterobacteriaceae*) is a gram-negative pathogenic bacterium that can invade, disrupt and destroy the intestinal epithelial

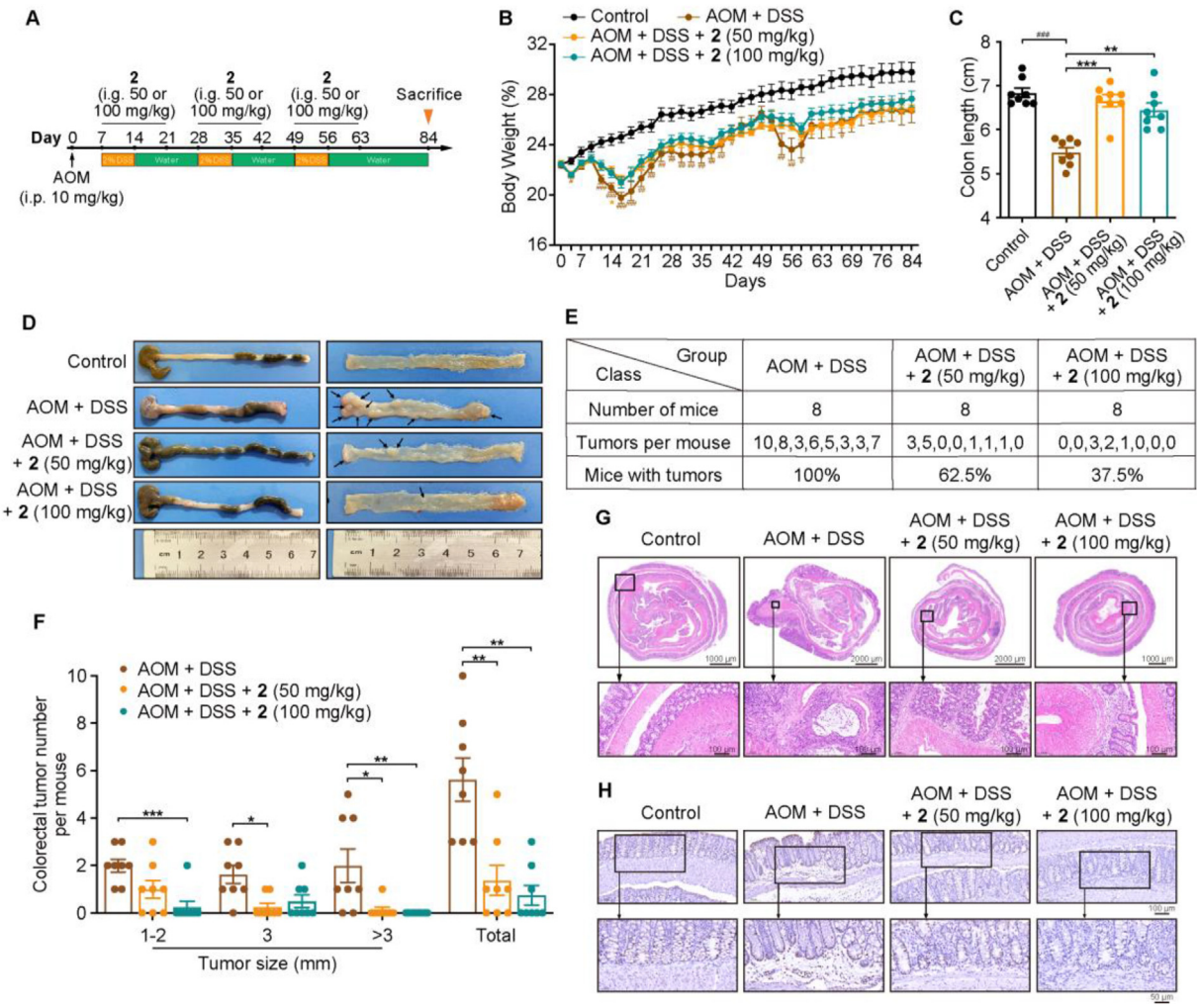

Figure 9 5*S*-Heudelotinone (**2**) reduces colonic tumorigenesis in a mouse model of CAC. (A) Procedure for the AOM/DSS-induced establishment of the CAC model in C57BL/6J mice and 5*S*-heudelotinone (**2**) treatment. (B) Changes in the body weights of mice in the four groups (Control, AOM, 50 mg/kg 5*S*-heudelotinone (**2**) and 100 mg/kg 5*S*-heudelotinone (**2**)). (C) Statistical histogram of colon lengths in the different groups on Day 84. (D) Representative images of colon and colorectal tumors in the different groups on Day 84. (E) Summarized results of tumor numbers per mouse and numbers of mice with tumors in the different groups on Day 84. (F) Statistical analysis of the number and size distribution of colorectal tumors in the different groups on Day 84. (G) Representative images of H&E staining of histological sections of "Swiss rolls" from different groups. (H) Histological staining for Ki67 in colorectal tumors from the four groups of mice. Scale bars: 2000 μm, 1000 μm, 100 μm and 50 μm. $n = 8$. The data are presented as the mean ± SEM; arrows indicate colorectal tumors; *P* values are calculated by two-way ANOVA with Turkey's multiple comparisons test (B) and one-way ANOVA with Dunnett's T3 multiple comparisons test (C, F): $^{\#}P < 0.05$, $^{\#\#}P < 0.01$, $^{\#\#\#}P < 0.001$ (AOM group *vs*. Control group); $^{*}P < 0.05$, $^{**}P < 0.01$, $^{***}P < 0.001$ (5*S*-heudelotinone treatment groups *vs*. AOM group).

barrier[65]. Therefore, these pathogenic bacteria play important roles in driving the development of IBD. Our studies showed that *Shigella* (from the phylum *Proteobacteria* to the family *Enterobacteriaceae*) was the predominant bacterial genus in the DSS group, and 5*S*-heudelotinone (**2**) dramatically decreased the proportions of *Proteobacteria*, *Gammaproteobacteria*, *Enterobacteriaceae* and *Shigella* from 10.76%, 7.93%, 7.90% and 7.19% in the DSS group to 1.76%, 0.16%, 0.15% and 0.12%, respectively, and these proportions were maintained at 0.60%, 0.16%, 0.08% and 0.05% in the Control group. These results suggest that 5*S*-heudelotinone (**2**) may improve colitis by reducing the abundance of harmful bacteria.

Conversely, some probiotic bacteria exert protective effects. S24-7, a family of common commensal bacteria in humans, has been shown to be effectively extinct in patients with diarrhea[66,67]. Similarly, the abundance of *Akkermansia*, a crucial organism that is located at the mucosal interface between the lumen and host cells, was decreased in patients and mice with colitis or CAC[68–70]. Previous studies revealed the protective effects of extracellular vesicles derived from *Akkermansia muciniphila* in DSS-induced colitis[71]. Further studies suggested that Amuc_1100, a specific outer membrane protein isolated from *A. muciniphila*, blunts colitis associated tumorigenesis through the expansion and activation of CTLs, which is demonstrated by TNF-α induction and PD-1 downregulation[69]. Another research discovered that Amuc_2172, an acetyltransferase of *A. muciniphila*, reprogrammed the colorectal tumor microenvironment (TME) with H3K14ac-induced HSP70 transcription and promoted CTL-related immune

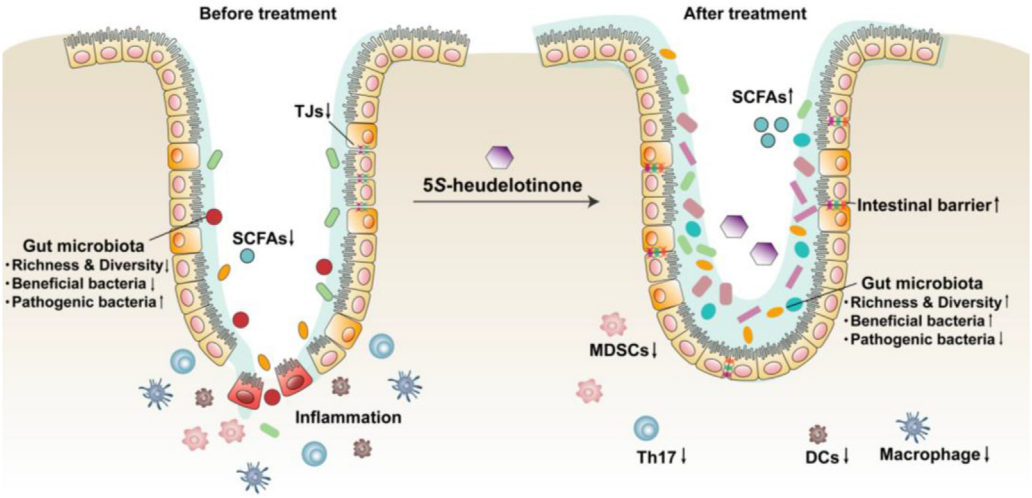

Figure 10 Proposed mechanisms by which 5*S*-heudelotinone (**2**) affects colitis.

response in the process of colorectal tumorigenesis[72]. Moreover, *Akkermansia* can produce SCFAs, including propionate and butyrate, thereby playing key roles in maintaining intestinal barrier function and host metabolism[73]. However, Matute et al. revealed that Intelectin-1 (ITLN1) decreased the thickness of the inner colonic mucus layer by binding and determining the localization of the mucin-degrading bacterium *A. muciniphila*[74]. Therefore, it seems that the pro-inflammatory effect of *A. muciniphila* occurs under certain conditions, which may be related to the factors such as the strain specificity, the sex of the host, the coexistence of other pathogenic bacteria, and differences in animal model[75−77]. In our study, the current evidence has demonstrated its potential value in preventing or treating IBD and CAC. In addition, *Odoribacter* is also a genus of SCFA-producing bacteria with anti-inflammatory properties that promote the alleviation of IBD. A decreased abundance of *Odoribacter* (member of the phylum *Bacteroidetes*) was verified in IBD samples. Intriguingly, *Odoribacter* appears to be related to metabolic health benefits when coupled with *Akkermansia*, particularly in the context of metabolism-related pathologies[78]. *Butyricicoccus pullicaecorum*, a producer of butyrate with probiotic potential, attenuates colitis in rats and strengthens the epithelial barrier in cells. Therefore, a promising probiotic candidate could be derived from the genus *Butyricicoccus*, as patients with IBD display lower fecal counts of these bacteria[79,80]. In this study, 5*S*-heudelotinone (**2**) significantly promoted the growth of S24-7, *Akkermansia*, and *Odoribacter* in fecal samples, and S24-7, *Odoribacter* and *Butyricicoccus* were the predominant members of the bacterial community after 5*S*-heudelotinone (**2**) treatment. Collectively, these results indicate that 5*S*-heudelotinone (**2**) increases the abundance of beneficial bacteria while simultaneously decreasing the proportion of pathogenic bacteria, thus alleviating DSS-induced colitis. Nonetheless, further studies are needed to determine how 5*S*-heudelotinone (**2**) affects these commensal bacteria in mice with IBD.

The gut microbiota not only directly affects intestinal homeostasis but also produces various metabolites (such as SCFAs, tryptophan catabolites, secondary bile acids (sBAs), branched-chain amino acids, and polyamines) to modulate the progression of intestinal diseases at both the metabolic and immunological levels[81]. Among these metabolites, SCFAs are a group of fatty acids with carbon numbers less than 6, and these SCFAs are metabolized from undigested carbohydrates by the gut microbiota in the intestinal tract. SCFAs primarily include acetate, propionate, butyrate, isobutyrate, valerate, isovalerate and caproate[17]. The significance of SCFAs in the body's inflammatory response has been extensively evidenced. The introduction of soluble fiber into the diet resulted in the decreased levels of pro-inflammatory cytokines such as IL-6, IL-8, and TNF[82]. The effects of SCFAs on the host's inflammatory response show conflicting results between pro-inflammatory and anti-inflammatory effects, possibly due to the different binding receptors and local concentrations[83]. Butyrate exerts anti-inflammatory effects by binding to and activating free fatty acid receptor 3 (FFAR3/GPR41), however, activation of FFAR2/3 by SCFAs further triggers the downstream mTOR, PI3K, ERK1/2, or MAPK signaling pathways, leading to pro-inflammatory effects[84−86]. Moreover, SCFAs also enter cells directly to regulate inflammation by inhibiting TNF expression, NF-κB signaling pathway, and histone deacetylation[87,88]. In addition, SCFAs are also capable of regulating inflammation by endothelial cells. SCFAs activate anti-inflammatory signaling pathways by inhibiting HDACs in endothelial cells. As an HDAC inhibitor, butyrate reduces the production of pro-inflammatory cytokines and oxidative stress, thereby inhibiting vascular inflammation and regulating endothelial function[89]. In summary, the primary mechanisms through which SCFAs regulate inflammation are cell signal transduction and histone deacetylase inhibition[23]. Reduced concentrations of SCFAs have been observed in patients with IBD and in experimental IBD mouse models[19]. Therefore, SCFAs play important roles in the occurrence and development of IBD. Currently, oral administration of exogenous butyrate has been used in clinical studies to treat IBD and improve intestinal inflammation[90,91]. Our data clearly demonstrate that 5*S*-heudelotinone (**2**) can effectively increase the levels of SCFAs, especially propionic acid and butyric acid, in fecal samples from IBD model mice.

It is widely accepted that SCFAs ameliorate inflammatory responses by modulating immune cells and enhancing intestinal barrier integrity[16]. SCFAs modulate the activity of innate immune cells, including macrophages, neutrophils, and DCs, thereby contributing to the function of the immune system[83]. Macrophages play a crucial role in maintaining gut homeostasis[20]. Previous

studies have demonstrated that butyric acid suppresses the production of inflammatory by intestinal macrophages is associated with the inhibition of HDAC activity. Moreover, butyric acid alters macrophage metabolism and increases their antibacterial activity by inhibiting mTOR kinase activity[92−94]. Similarly, butyrate also can boost the antibacterial capabilities of macrophages by inhibiting HDAC3[95]. In addition, SCFAs are essential regulators of macrophage polarization. Butyrate altered the metabolic behavior of macrophages to increase OXPHOS and also promoted alternative macrophage activation[96]. Another crucial component of the innate immune defenses is the neutrophil. SCFAs alter neutrophils recruitment by regulate the production of inflammatory mediators such as TNF-α, IL-17, CXCL1 and CXCL8[97−99]. Moreover, activation of FFAR2 by SCFAs in neutrophils has been demonstrated to induce their chemotaxis[100,101]. DCs are also part of the host defense and play an important role in the induction and maintenance of immune tolerance under homeostatic conditions[102]. Butyrate can inhibit the maturation of DCs when exposed to various inflammatory stimulation, and it can also alter the antigen capture capacity by modulating the differentiation and functions of DCs. Moreover, butyrate modulates the production of cytokines and chemokines, such as IL-23, IL-10 and IL-12, that are secreted by DCs[103−106]. Wang et al. revealed that butyrate functioned as a histone deacetylase (HDAC) inhibitor, impeding the functional differentiation of human monocyte-derived DCs[107]. In conclusion, it is well-established that SCFAs, especially butyrate, modulate different aspects of innate immune response. Additionally, SCFAs also affect the polarization and activation of Th1, Th2, and Th17 cells by inhibiting HDACs, promote colonic Treg cell differentiation and increase the number of Treg cells[16].

In addition to regulating both innate and adaptive immune cells, SCFAs, especially butyrate, are the most important components for maintaining intestinal epithelial integrity and restoring barrier function[17]. The intestinal physical barrier, which is composed of intestinal epithelial cells (IECs) and the mucus layer, is the first line of defense against bacterial toxins and harmful pathogens[108]. TJs are multiprotein complexes that form a continuous intercellular barrier between IECs and maintain selectively permeable barriers, which are needed to regulate the transport of macromolecules and prevent the infiltration of pathogens from the intestinal lumen. TJs are primarily composed of transmembrane proteins (such as Claudins and Occludins) and junctional adhesion molecules (JAMs), which are the main factors that regulate paracellular permeability. When the TJ barrier is disrupted, paracellular permeability is significantly increased, leading to the penetration of macromolecules and pathogenic bacteria into the lamina propria and then resulting in disordered mucosal immune responses and inflammation. Studies have reported that the TJs in IBD patients are disrupted, indicating that the integrity of the intestinal barrier is impaired; this can lead to or promote the progression of IBD[108]. Therefore, restoring intestinal barrier integrity may be an effective strategy for the prevention and treatment of IBD. In our IBD model that was treated with 5*S*-heudelotinone (**2**), both immune cells and the epithelial barrier were strongly affected, and the gut microbiota played a crucial role in this process, which was verified in an ABX mouse model.

5. Conclusions

In summary, we describe for the first time a concise and efficient method for the synthesis of a racemate of heudelotinone and investigate the effect and underlying mechanisms of 5*S*-heudelotinone (**2**) on experimental colitis and CAC. By targeting the gut microbiota, 5*S*-heudelotinone (**2**) increases the levels of SCFAs, thereby promoting a balanced immune response and a robust intestinal barrier for the prevention and treatment of IBD. This work highlights that utilizing reagents to modulate the gut microbiota is a safe and efficient strategy, and this study demonstrates that 5*S*-heudelotinone (**2**) is a promising candidate for the prevention and treatment of IBD-related diseases.

Acknowledgments

This work was financially supported by the National Natural Science Foundation of China (82273794 to Yue Chen and 82073879 to Jing Li.), the Natural Science Foundation of Tianjin (21JCYBJC00190 to Jing Li and 20JCYBJC01000 to Yue Chen) and the Postdoctoral Science Foundation of China (2021M701791).

Author contributions

Qing Meng, Jianshuang Guo, Quan Zhang, Yue Chen and Jing Li devised the project. Qing Meng carried out the experimental work and analyzed the data. Qing Meng and Jin Zhang synthesized the compounds. Qing Meng, Yang Liu, Ke Lv, Mingyue Li, Xirui Cheng and Xiaoguang Huo carried out the experimental work. Shenghua Chen and Qing Meng finished Fig. 10. Qing Meng, Quan Zhang, Yue Chen and Jing Li wrote the manuscript.

Conflicts of interest

The authors declare no conflicts of interest.

Appendix A. Supporting information

Supporting data to this article can be found online at https://doi.org/10.1016/j.apsb.2024.02.020.

References

1. Abraham C. Inflammatory bowel disease. *N Engl J Med* 2009;**361**:2066−78.
2. Molodecky NA, Soon IS, Rabi DM, Ghali WA, Ferris M, Chernoff G, et al. Increasing incidence and prevalence of the inflammatory bowel diseases with time, based on systematic review. *Gastroenterology* 2012;**142**:46−54.
3. Ullman TA, Itzkowitz SH. Intestinal inflammation and cancer. *Gastroenterology* 2011;**140**:1807−16.
4. Fantini MC, Guadagni I. From inflammation to colitis-associated colorectal cancer in inflammatory bowel disease: pathogenesis and impact of current therapies. *Dig Liver Dis* 2021;**53**:558−65.
5. Ng SC, Shi HY, Hamidi N, Underwood FE, Tang W, Benchimol EI, et al. Worldwide incidence and prevalence of inflammatory bowel disease in the 21st century: a systematic review of population-based studies. *Lancet* 2017;**390**:2769−78.
6. Ananthakrishnan AN. Epidemiology and risk factors for IBD. *Nat Rev Gastroenterol Hepatol* 2015;**12**:205−17.
7. Lee M, Chang EB. Inflammatory bowel diseases (IBD) and the microbiome−searching the crime scene for clues. *Gastroenterology* 2021;**160**:524−37.
8. Cai Z, Wang S, Li J. Treatment of inflammatory bowel disease: a comprehensive review. *Front Med* 2021;**8**:765474.
9. Manichanh C, Borruel N, Casellas F, Guarner F. The gut microbiota in IBD. *Nat Rev Gastroenterol Hepatol* 2012;**9**:599−608.

10. Federici S, Kredo-Russo S, Valdés-Mas R, Kviatcovsky D, Weinstock E, Matiuhin Y, et al. Targeted suppression of human IBD-associated gut microbiota commensals by phage consortia for treatment of intestinal inflammation. *Cell* 2022;**185**:2879−98.
11. Franzosa EA, Sirota-Madi A, Avila-Pacheco J, Fornelos N, Haiser HJ, Reinker S, et al. Gut microbiome structure and metabolic activity in inflammatory bowel disease. *Nat Microbiol* 2018;**4**:293−305.
12. Manichanh C. Reduced diversity of faecal microbiota in Crohn's disease revealed by a metagenomic approach. *Gut* 2006;**55**:205−11.
13. Kostic AD, Xavier RJ, Gevers D. The microbiome in inflammatory bowel disease: current status and the future ahead. *Gastroenterology* 2014;**146**:1489−99.
14. Yang W, Cong Y. Gut microbiota-derived metabolites in the regulation of host immune responses and immune-related inflammatory diseases. *Cell Mol Immunol* 2021;**18**:866−77.
15. Cai J, Sun L, Gonzalez FJ. Gut microbiota-derived bile acids in intestinal immunity, inflammation, and tumorigenesis. *Cell Host Microbe* 2022;**30**:289−300.
16. Deleu S, Machiels K, Raes J, Verbeke K, Vermeire S. Short chain fatty acids and its producing organisms: an overlooked therapy for IBD?. *EBioMedicine* 2021;**66**:103293.
17. Liu P, Wang Y, Yang G, Zhang Q, Meng L, Xin Y, et al. The role of short-chain fatty acids in intestinal barrier function, inflammation, oxidative stress, and colonic carcinogenesis. *Pharmacol Res* 2021;**165**:105420.
18. Parada Venegas D, De La Fuente MK, Landskron G, González MJ, Quera R, Dijkstra G, et al. Short chain fatty acids (SCFAs)-mediated gut epithelial and immune regulation and its relevance for inflammatory bowel diseases. *Front Immunol* 2019;**10**:277.
19. Gonçalves P, Araújo JR, Di Santo JP. A cross-talk between microbiota-derived short-chain fatty acids and the host mucosal immune system regulates intestinal homeostasis and inflammatory bowel disease. *Inflamm Bowel Dis* 2018;**24**:558−72.
20. Hegarty LM, Jones GR, Bain CC. Macrophages in intestinal homeostasis and inflammatory bowel disease. *Nat Rev Gastroenterol Hepatol* 2023;**20**:538−53.
21. Chang JT. Pathophysiology of inflammatory bowel diseases. *N Engl J Med* 2020;**383**:2652−64.
22. Pan X, Zhu Q, Pan LL, Sun J. Macrophage immunometabolism in inflammatory bowel diseases: from pathogenesis to therapy. *Pharmacol Therapeut* 2022;**238**:108176.
23. Zhang Z, Zhang H, Chen T, Shi L, Wang D, Tang D. Regulatory role of short-chain fatty acids in inflammatory bowel disease. *Cell Commun Signal* 2022;**20**:64.
24. Dalile B, Van Oudenhove L, Vervliet B, Verbeke K. The role of short-chain fatty acids in microbiota−gut−brain communication. *Nat Rev Gastroenterol Hepatol* 2019;**16**:461−78.
25. Britton GJ, Contijoch EJ, Mogno I, Vennaro OH, Llewellyn SR, Ng R, et al. Microbiotas from humans with inflammatory bowel disease alter the balance of gut Th17 and RORγt+ regulatory T cells and exacerbate colitis in mice. *Immunity* 2019;**50**:212−24.
26. Hou G, Bishu S. Th17 cells in inflammatory bowel disease: an update for the clinician. *Inflamm Bowel Dis* 2020;**26**:653−61.
27. Jiang P, Zheng C, Xiang Y, Malik S, Su D, Xu G, et al. The involvement of TH17 cells in the pathogenesis of IBD. *Cytokine Growth Factor Rev* 2023;**69**:28−42.
28. Ueno A, Jeffery L, Kobayashi T, Hibi T, Ghosh S, Jijon H. Th17 plasticity and its relevance to inflammatory bowel disease. *J Autoimmun* 2018;**87**:38−49.
29. Clough JN, Omer OS, Tasker S, Lord GM, Irving PM. Regulatory T-cell therapy in Crohn's disease: challenges and advances. *Gut* 2020;**69**:942−52.
30. Smith PM, Howitt MR, Panikov N, Michaud M, Gallini CA, Bohlooly-Y M, et al. The microbial metabolites, short-chain fatty acids, regulate colonic Treg cell homeostasis. *Science* 2013;**341**:569−73.
31. Omenetti S, Pizarro TT. The Treg/Th17 axis: a dynamic balance regulated by the gut microbiome. *Front Immunol* 2015;**6**:639.
32. Lee G. The balance of Th17 *versus* Treg cells in autoimmunity. *Int J Mol Sci* 2018;**19**:730.
33. Gasaly N, De Vos P, Hermoso MA. Impact of bacterial metabolites on gut barrier function and host immunity: a focus on bacterial metabolism and its relevance for intestinal inflammation. *Front Immunol* 2021;**12**:658354.
34. Lee SH. Intestinal permeability regulation by tight junction: implication on inflammatory bowel diseases. *Int Res* 2015;**13**:11.
35. Zuo L, Kuo WT, Turner JR. Tight junctions as targets and effectors of mucosal immune homeostasis. *Cell Mol Gastroenter* 2020;**10**:327−40.
36. Zhu L, Han J, Li L, Wang Y, Li Y, Zhang S. Claudin family participates in the pathogenesis of inflammatory bowel diseases and colitis-associated colorectal cancer. *Front Immunol* 2019;**10**:1441.
37. Kelly CJ, Zheng L, Campbell EL, Saeedi B, Scholz CC, Bayless AJ, et al. Crosstalk between microbiota-derived short-chain fatty acids and intestinal epithelial HIF augments tissue barrier function. *Cell Host Microbe* 2015;**17**:662−71.
38. Wang HB, Wang PY, Wang X, Wan YL, Liu YC. Butyrate enhances intestinal epithelial barrier function *via* up-regulation of tight junction protein claudin-1 transcription. *Dig Dis Sci* 2012;**57**:3126−35.
39. Zheng L, Kelly CJ, Battista KD, Schaefer R, Lanis JM, Alexeev EE, et al. Microbial-derived butyrate promotes epithelial barrier function through IL-10 receptor-dependent repression of claudin-2. *J Immunol* 2017;**199**:2976−84.
40. Liu T, Ning Z, Liu P, Gao H. Cassane diterpenoid ameliorates dextran sulfate sodium-induced experimental colitis by regulating gut microbiota and suppressing tryptophan metabolism. *Front Immunol* 2023;**13**:1045901.
41. Zhang S, Luo H, Sun S, Zhang Y, Ma J, Lin Y, et al. *Salvia miltiorrhiza* Bge. (Danshen) for inflammatory bowel disease: clinical evidence and network pharmacology-based strategy for developing supplementary medical application. *Front Pharmacol* 2022;**12**:741871.
42. Tu WC, Zhao YX, Yang CL, Zhang XJ, Li XL, Sakah KJ, et al. Abietane diterpenoids from *Orthosiphon wulfenioides* with NLRP3 inflammasome inhibitory activity. *Bioorg Chem* 2023;**136**:106534.
43. Zheng JH, Lin SR, Tseng FJ, Tsai MJ, Lue SI, Chia YC, et al. Clerodane diterpene ameliorates inflammatory bowel disease and potentiates cell apoptosis of colorectal cancer. *Biomolecules* 2019;**9**:762.
44. Kim C, Le D, Lee M. Diterpenoids isolated from *Podocarpus macrophyllus* inhibited the inflammatory mediators in LPS-induced HT-29 and RAW 264.7 cells. *Molecules* 2021;**26**:4326.
45. Feng Z, Cao J, Zhang Q, Lin L. The drug likeness analysis of anti-inflammatory clerodane diterpenoids. *Chin Med* 2020;**15**:126.
46. Esquivel B. Rearranged clerodane and abietane derived diterpenoids from American *Salvia* species. *Nat Prod Commun* 2008;**3**:1934578X0800300.
47. Kimbu SF, Keumedjio F, Sondengam LB, Connolly JD. Two dinorditerpenoids from *Ricinodendron heudelotii*. *Phytochemistry* 1991;**30**:619−21.
48. Chao CH, Cheng JC, Shen DY, Huang HC, Wu YC, Wu TS. Terpenoids from *Flueggea virosa* and their anti-hepatitis C virus activity. *Phytochemistry* 2016;**128**:60−70.
49. Zhu Q, Tang CP, Ke CQ, Li XQ, Liu J, Gan LS, et al. Constituents of *Trigonostemon chinensis*. *J Nat Prod* 2010;**73**:40−4.
50. Ravindranath N, Ravinder Reddy M, Ramesh C, Ramu R, Prabhakar A, Jagadeesh B, et al. New lathyrane and podocarpane diterpenoids from *Jatropha curcas*. *Chem Pharm Bull* 2004;**52**:608−11.
51. Yang B, Chen GY, Song XP, Yang LQ, Wu XY, Han CR, et al. Five new degraded diterpenoids from *Trigonostemon xyphophylloides*. *Bioorg Med Chem Lett* 2013;**23**:5748−51.
52. Zhu JY, Zhang CY, Dai JJ, Rahman K, Zhang H. Diterpenoids with thioredoxin reductase inhibitory activities from *Jatropha multifida*. *Nat Prod Res* 2017;**31**:2753−8.

53. Xu JJ, Fan JT, Zeng GZ, Tan NH. A new tetracyclic diterpene from *Jatropha curcas*. *Helv Chim Acta* 2011;**94**:842−6.
54. Neufert C, Heichler C, Brabletz T, Scheibe K, Boonsanay, Greten FR, et al. Inducible mouse models of colon cancer for the analysis of sporadic and inflammation-driven tumor progression and lymph node metastasis. *Nat Protoc* 2021;**16**:61−85.
55. Danishefsky S, Kitahara T. Useful diene for the Diels−Alder reaction. *J Am Chem Soc* 1974;**96**:7807−8.
56. Nicolaou KC, Snyder SA, Montagnon T, Vassilikogiannakis G. The Diels−Alder reaction in total synthesis. *Angew Chem Int Ed* 2002;**41**: 1668−98.
57. Liu YP, Wen Q, Hu S, Ma YL, Jiang ZH, Tang JY, et al. Structurally diverse diterpenoids from *Trigonostemon howii*. *Nat Prod Res* 2019; **33**:1169−74.
58. Ma J, Piao X, Mahfuz S, Long S, Wang J. The interaction among gut microbes, the intestinal barrier and short chain fatty acids. *Anim Nutr* 2022;**9**:159−74.
59. Simmons EM, Sarpong R. Structure, biosynthetic relationships and chemical synthesis of the icetexane diterpenoids. *Nat Prod Rep* 2009; **26**:1195.
60. Huang JD, Zhang C, Xu WJ, Lian CL, Liu XM, Wang CF, et al. New lathyrane diterpenoids with anti-inflammatory activity isolated from the roots of *Jatropha curcas* L. *J Ethnopharmacol* 2021;**268**:113673.
61. Kamran S, Sinniah A, Abdulghani MAM, Alshawsh MA. Therapeutic potential of certain terpenoids as anticancer agents: a scoping review. *Cancers* 2022;**14**:1100.
62. Ni J, Wu GD, Albenberg L, Tomov VT. Gut microbiota and IBD: causation or correlation?. *Nat Rev Gastroenterol Hepatol* 2017;**14**: 573−84.
63. Nomura K, Ishikawa D, Okahara K, Ito S, Haga K, Takahashi M, et al. Bacteroidetes species are correlated with disease activity in ulcerative colitis. *J Clin Med* 2021;**10**:1749.
64. Mukhopadhya I, Hansen R, El-Omar EM, Hold GL. IBD—what role do Proteobacteria play?. *Nat Rev Gastroenterol Hepatol* 2012;**9**: 219−30.
65. Andoh A, Imaeda H, Aomatsu T, Inatomi O, Bamba S, Sasaki M, et al. Comparison of the fecal microbiota profiles between ulcerative colitis and Crohn's disease using terminal restriction fragment length polymorphism analysis. *J Gastroenterol* 2011;**46**:479−86.
66. Lagkouvardos I, Lesker TR, Hitch TCA, Gálvez EJC, Smit N, Neuhaus K, et al. Sequence and cultivation study of Muribaculaceae reveals novel species, host preference, and functional potential of this yet undescribed family. *Microbiome* 2019;**7**:28.
67. Rooks MG, Veiga P, Wardwell-Scott LH, Tickle T, Segata N, Michaud M, et al. Gut microbiome composition and function in experimental colitis during active disease and treatment-induced remission. *ISME J* 2014;**8**:1403−17.
68. Bian X, Wu W, Yang L, Lv L, Wang Q, Li Y, et al. Administration of *Akkermansia muciniphila* ameliorates dextran sulfate sodium-induced ulcerative colitis in mice. *Front Microbiol* 2019;**10**:2259.
69. Wang L, Tang L, Feng Y, Zhao S, Han M, Zhang C, et al. A purified membrane protein from *Akkermansia muciniphila* or the pasteurised bacterium blunts colitis associated tumourigenesis by modulation of $CD8^+$ T cells in mice. *Gut* 2020;**69**:1988−97.
70. Collins D, Hogan AM, Winter DC. Microbial and viral pathogens in colorectal cancer. *Lancet Oncol* 2011;**12**:504−12.
71. Kang C, Ban M, Choi EJ, Moon HG, Jeon JS, Kim DK, et al. Extracellular vesicles derived from gut microbiota, especially *Akkermansia muciniphila*, protect the progression of dextran sulfate sodium-induced colitis. *PLoS One* 2013;**8**:e76520.
72. Jiang Y, Xu Y, Zheng C, Ye L, Jiang P, Malik S, et al. Acetyltransferase from *Akkermansia muciniphila* blunts colorectal tumourigenesis by reprogramming tumour microenvironment. *Gut* 2023;**72**:1308−18.
73. Li W, Zhang L, Xu Q, Yang W, Zhao J, Ren Y, et al. Taxifolin alleviates DSS-induced ulcerative colitis by acting on gut microbiome to produce butyric acid. *Nutrients* 2022;**14**:1069.
74. Matute JD, Duan J, Flak MB, Griebel P, Tascon-Arcila JA, Doms S, et al. Intelectin-1 binds and alters the localization of the mucus barrier-modifying bacterium *Akkermansia muciniphila*. *J Exp Med* 2023;**220**:e20211938.
75. Li M, Wu Y, Hu Y, Zhao L, Zhang C. Initial gut microbiota structure affects sensitivity to DSS-induced colitis in a mouse model. *Sci China Life Sci* 2018;**61**:762−9.
76. Zhang T, Ji X, Lu G, Zhang F. The potential of *Akkermansia muciniphila* in inflammatory bowel disease. *Appl Microbiol Biotechnol* 2021;**105**:5785−94.
77. Kim S, Shin YC, Kim TY, Kim Y, Lee YS, Lee SH, et al. Mucin degrader *Akkermansia muciniphila* accelerates intestinal stem cell-mediated epithelial development. *Gut Microb* 2021;**13**:1892441.
78. Hiippala K, Barreto G, Burrello C, Diaz-Basabe A, Suutarinen M, Kainulainen V, et al. Novel *Odoribacter splanchnicus* strain and its outer membrane vesicles exert immunoregulatory effects *in vitro*. *Front Microbiol* 2020;**11**:575455.
79. Marteau P. Butyrate-producing bacteria as pharmabiotics for inflammatory bowel disease. *Gut* 2013;**62**:1673.
80. Geirnaert A, Steyaert A, Eeckhaut V, Debruyne B, Arends JBA, Van Immerseel F, et al. *Butyricicoccus pullicaecorum*, a butyrate producer with probiotic potential, is intrinsically tolerant to stomach and small intestine conditions. *Anaerobe* 2014;**30**:70−4.
81. Lavelle A, Sokol H. Gut microbiota-derived metabolites as key actors in inflammatory bowel disease. *Nat Rev Gastroenterol Hepatol* 2020;**17**:223−37.
82. Macfarlane S, Cleary S, Bahrami B, Reynolds N, Macfarlane GT. Synbiotic consumption changes the metabolism and composition of the gut microbiota in older people and modifies inflammatory processes: a randomised, double-blind, placebo-controlled crossover study. *Aliment Pharmacol Ther* 2013;**38**:804−16.
83. Yao Y, Cai X, Fei W, Ye Y, Zhao M, Zheng C. The role of short-chain fatty acids in immunity, inflammation and metabolism. *Crit Rev Food Sci* 2022;**62**:1−12.
84. Seljeset S, Siehler S. Receptor-specific regulation of ERK1/2 activation by members of the "free fatty acid receptor" family. *J Recept Signal Transduction* 2012;**32**:196−201.
85. Thorburn AN, Macia L, Mackay CR. Diet, metabolites, and "Western-lifestyle" inflammatory diseases. *Immunity* 2014;**40**:833−42.
86. Sun M, Wu W, Liu Z, Cong Y. Microbiota metabolite short chain fatty acids, GPCR, and inflammatory bowel diseases. *J Gastroenterol* 2017;**52**:1−8.
87. Aoyama M, Kotani J, Usami M. Butyrate and propionate induced activated or non-activated neutrophil apoptosis *via* HDAC inhibitor activity but without activating GPR-41/GPR-43 pathways. *Nutrition* 2010;**26**:653−61.
88. Chang PV, Hao L, Offermanns S, Medzhitov R. The microbial metabolite butyrate regulates intestinal macrophage function *via* histone deacetylase inhibition. *Proc Natl Acad Sci USA* 2014;**111**: 2247−52.
89. Didonna A, Opal P. The promise and perils of HDAC inhibitors in neurodegeneration. *Ann Clin Transl Neurol* 2015;**2**:79−101.
90. Pietrzak A, Banasiuk M, Szczepanik M, Borys-Iwanicka A, Pytrus T, Walkowiak J, et al. Sodium butyrate effectiveness in children and adolescents with newly diagnosed inflammatory bowel diseases—randomized placebo-controlled multicenter trial. *Nutrients* 2022;**14**:3283.
91. Wang R, Cao S, Bashir MEH, Hesser LA, Su Y, Hong SMC, et al. Treatment of peanut allergy and colitis in mice *via* the intestinal release of butyrate from polymeric micelles. *Nat Biomed Eng* 2022;**7**: 38−55.
92. Schulthess J, Pandey S, Capitani M, Rue-Albrecht KC, Arnold I, Franchini F, et al. The short chain fatty acid butyrate imprints an antimicrobial program in macrophages. *Immunity* 2019;**50**: 432−445.e7.
93. Flemming A. Butyrate boosts microbicidal macrophages. *Nat Rev Immunol* 2019;**19**. 135−135.

94. Lobel L, Garrett WS. Butyrate makes macrophages "go nuclear" against bacterial pathogens. *Immunity* 2019;**50**:275−8.
95. Zhao C, Bao L, Zhao Y, Wu K, Qiu M, Feng L, et al. A fiber-enriched diet alleviates Staphylococcus aureus-induced mastitis by activating the HDAC3-mediated antimicrobial program in macrophages *via* butyrate production in mice. *PLoS Pathog* 2023;**19**:1−21.
96. Scott NA, Andrusaite A, Andersen P, Lawson M, Alcon-Giner C, Leclaire C, et al. Antibiotics induce sustained dysregulation of intestinal T cell immunity by perturbing macrophage homeostasis. *Sci Transl Med* 2018;**10**:eaao4755.
97. Singh N, Gurav A, Sivaprakasam S, Brady E, Padia R, Shi H, et al. Activation of Gpr109a, receptor for niacin and the commensal metabolite butyrate, suppresses colonic inflammation and carcinogenesis. *Immunity* 2014;**40**:128−39.
98. Vinolo MAR, Rodrigues HG, Hatanaka E, Hebeda CB, Farsky SHP, Curi R. Short-chain fatty acids stimulate the migration of neutrophils to inflammatory sites. *Clin Sci* 2009;**117**:331−8.
99. Vinolo MAR, Rodrigues HG, Hatanaka E, Sato FT, Sampaio SC, Curi R. Suppressive effect of short-chain fatty acids on production of proinflammatory mediators by neutrophils. *J Nutr Biochem* 2011;**22**:849−55.
100. Le Poul E, Loison C, Struyf S, Springael JY, Lannoy V, Decobecq ME, et al. Functional characterization of human receptors for short chain fatty acids and their role in polymorphonuclear cell activation. *J Biol Chem* 2003;**278**:25481−9.
101. Sina C, Gavrilova O, Förster M, Till A, Derer S, Hildebrand F, et al. G protein-coupled receptor 43 is essential for neutrophil recruitment during intestinal inflammation. *J Immunol* 2009;**183**:7514−22.
102. Zanna MY, Yasmin AR, Omar AR, Arshad SS, Mariatulqabtiah AR, Nur-Fazila SH, et al. Review of dendritic cells, their role in clinical immunology, and distribution in various animal species. *Indian J Manag Sci* 2021;**22**:8044.
103. Corrêa-Oliveira R, Fachi JL, Vieira A, Sato FT, Vinolo MAR. Regulation of immune cell function by short-chain fatty acids. *Clin Transl Immunology* 2016;**5**:e73.
104. Millard AL, Mertes PM, Ittelet D, Villard F, Jeannesson P, Bernard J. Butyrate affects differentiation, maturation and function of human monocyte-derived dendritic cells and macrophages. *Clin Exp Immunol* 2002;**130**:245−55.
105. Liu L, Li L, Min J, Wang J, Wu H, Zeng Y, et al. Butyrate interferes with the differentiation and function of human monocyte-derived dendritic cells. *Cell Immunol* 2012;**277**:66−73.
106. Nastasi C, Fredholm S, Willerslev-Olsen A, Hansen M, Bonefeld CM, Geisler C, et al. Butyrate and propionate inhibit antigen-specific $CD8^+$ T cell activation by suppressing IL-12 production by antigen-presenting cells. *Sci Rep* 2017;**7**:14516.
107. Wang B, Morinobu A, Horiuchi M, Liu J, Kumagai S. Butyrate inhibits functional differentiation of human monocyte-derived dendritic cells. *Cell Immunol* 2008;**253**:54−8.
108. Peterson LW, Artis D. Intestinal epithelial cells: regulators of barrier function and immune homeostasis. *Nat Rev Immunol* 2014;**14**:141−53.